This is a preprint, the final version is subject to change, of the American Mineralogist (MSA)
Cite as Authors (Year) Title. American Mineralogist, in press.
DOI: https://doi.org/10.2138/am-2019-7099

Revision 2 (for Ms. Ref. No.: 7099R1)

Thermal diffusivity and thermal conductivity of granitoids at 283–988 K and 0.3–1.5 GPa

Huangfei Fu[1, 2], Baohua Zhang[1*], Jianhua Ge[1, 2], Zili Xiong[1, 2] Shuangmeng Zhai[1], Shuangming Shan[1], Heping Li[1]

[1]Key Laboratory for High-Temperature and High-Pressure Study of the Earth's Interior, Institute of Geochemistry, Chinese Academy of Sciences, Guiyang, Guizhou 550081, China

[2]University of Chinese Academy of Sciences, Beijing 100049, China

* Author to whom correspondence should be addressed.

Dr. Baohua Zhang

Key Laboratory for High-Temperature and High-Pressure Study of the Earth's Interior, Institute of Geochemistry, Chinese Academy of Sciences, Guiyang, Guizhou 550081, China

E-mail: zhangbaohua@vip.gyig.ac.cn

Fax: +86-851-5895768

Tel: +86-851-5895768

This is a preprint, the final version is subject to change, of the American Mineralogist (MSA)
Cite as Authors (Year) Title. American Mineralogist, in press.
DOI: https://doi.org/10.2138/am-2019-7099

ABSTRACT

The thermal diffusivity and thermal conductivity of four natural granitoid samples were simultaneously measured at high pressures (up to 1.5 GPa) and temperatures (up to 988 K) in a multi-anvil apparatus using the transient plane-source method. Experimental results show that thermal diffusivity and thermal conductivity decreased with increasing temperature (< 600 K) and remain constant or slightly increase at a temperature range from 700 to 988 K. Thermal conductivity decreases 23%–46% between room temperature and 988 K, suggesting a typical manifestations of phonon conductivity. At higher temperatures, an additional radiative contribution is observed in four natural granitoids. Pressure exerts a weak but clear and positive influence on thermal transport properties. The thermal diffusivity and thermal conductivity of all granitoid samples exhibit a positive linear dependence on quartz content, whereas a negative linear dependence on plagioclase content appears. Combining these results with the measured densities, thermal diffusivity and thermal conductivity, and specific heat capacities of end-member minerals, the thermal diffusivity and thermal conductivity and bulk heat capacities for granitoids predicted from several mixing models are found to be consistent with the present experimental data. Furthermore, by combining the measured thermal properties and surface heat flows, calculated geotherms suggest that the presence of partial melting induced by muscovite or biotite dehydration likely occurs in the upper -middle crust of southern Tibet. This finding provides new insights into the origin of low-velocity and high-conductivity anomaly

zones revealed by geophysical observations in this region.

Keywords: thermal diffusivity, thermal conductivity, granitoid, crust

INTRODUCTION

Granite is one of the most abundant rock types of the continental crust. Heat transfer and temperature distribution in the crust is strongly influenced by the thermal properties of granite (e.g., Pollack and Chapman 1977; Clauser 2009; Whittington et al. 2009; Clark et al. 2011). Therefore, comprehensive knowledge of thermal transport properties (thermal diffusivity and thermal conductivity) of granites at elevated temperatures and pressures is essential to evaluate or quantitatively simulate many geodynamic processes. These processes include magmatism, metamorphism, and earthquakes occurring within the crust (e.g., Branlund et al. 2000; Annen et al. 2005; Whittington et al. 2009; Nabelek et al. 2010; Sawyer et al. 2011), as well as the thermal structure and thermal evolution of the earth (McKenzie et al. 2005; Clauser 2009; Furlong and Chapman 2013).

Over the past few decades, various experimental approaches have been developed to measure the thermal properties of diverse rock types and rock-forming minerals at high temperatures and high pressures (e.g., Birch and Clark 1940; Kanamori et al. 1968; Durhum et al. 1987; Seipold 1992; Maqsood et al. 2004; Ray et al. 2006; Abdulagatov et al. 2009; Whittington et al. 2009; Miao et al. 2014; Zhao et al. 2016). Results indicate that the thermal diffusivity and thermal conductivity of minerals and rocks are closely associated with mineral composition, porosity, texture,

and density. For crystalline rocks with relatively homogeneous textures and low porosities, for example, mineral composition dominates thermal transport properties (Höfer and Schilling 2002). In general, the thermal conductivity of rocks and minerals decreases and increases with increasing temperature and pressure, respectively. Seipold (1992) studied the pressure and temperature dependence of the thermal diffusivity of granites and some high-grade metamorphic rocks using a pulse technique and calculated the thermal conductivity of granites by taking into account the temperature dependence of specific heat values derived from literature data. He found that, within the crust, thermal properties are dominated by the influence of temperature, whereas the effect of pressure becomes more apparent at the depth of the upper mantle. Maqsood et al. (2004) reported the chemical composition, density, porosity, specific gravity, and thermal transport properties of 17 granite samples. Their studies found no correlation between the temperature dependence of the thermal transport behavior on porosity, chemical composition, and density, in part, because of a narrow range of temperatures studied 253–333 K.

Although previous studies provided meaningful insights into the thermal transport properties of various rock types, especially granites, most experimental measurements of the thermal properties of rock materials were performed at high pressures (< 0.5 GPa) but low temperatures (< 850 K) and vice versa. For estimations of crustal temperatures from heat flow and geothermal gradient data, knowledge of the temperature and pressure dependence of the thermal conductivity of granites is needed to allow extrapolation to greater depths. To date, studies of the combined

effect of high temperature and pressure on the thermal properties of granites remain scarce.

In this study, the thermal diffusivity and thermal conductivity of four natural granitoids with different compositions, are simultaneously measured under high pressure (0.3–1.5 GPa) and high temperature (283–988 K) using the transient plane-source method (Dzhavadov 1975; Osako et al. 2004; Miao et al. 2014) in a multi-anvil apparatus. Given the present experimental results, we discuss the effects of temperature, pressure, and mineral constituents on the thermal transport properties of granite. Furthermore, the geothermal gradient of the granitic upper crust of southern Tibet is reasonably evaluated by combining this newly acquired data with regional heat flow data and provides new constraints on the possibility of partial melting within the Tibetan crust.

EXPERIMENTAL METHODS

Rock samples and preparation

Four natural granitoids were investigated in this study, including grandiorite (DL-1) from the R'azhai area, southern Tibet, monzogranite and syenogranite (GCH-1, GCH-2) from the Guichi area, Anhui Province, and alkaline granite (TLP-1) from the Qingyang area, Gansu Province, China (Tables 1). Several thin sections were prepared and examined optically to identify the dominant minerals in the rocks and evaluate alteration and textures. Modal mineral abundances were determined by point counting on a series of thin sections of each sample (Table 1). The primary mineralogy of the

114 samples includes quartz (19–32 vol%), alkali-feldspar (16–60 vol%), plagioclase
115 (6–52 vol%), and small amounts of biotite, amphibole, and accessory minerals (garnet,
116 rutile, titanite). Detailed features are shown in Fig. 1. All collected samples were
117 relatively fresh (except for slight alteration of some feldspars that were locally
118 replaced by sericite and epidote); fine-grained to medium-to-coarse grained; and with
119 no preferred orientation of mineral grains. Major elements of each granite sample
120 were determined by X-ray fluorescence spectrometry (Supplementary Table 1). The
121 accelerating potential and beam current used were 20 kV and 22 nA, respectively.
122 Samples without visible cracks or heterogeneity were cored and cut into disks 10
123 mm in diameter and ~1.5 mm in thickness. The surface of all specimens was polished
124 with sandpaper and then with 1 μm diamond powder to minimize contact resistance.
125 Samples were cleaned in acetone and ethanol using an ultrasonic cleaner and dried in
126 a vacuum oven at 473 K for 24 h to remove any possible absorbed water before
127 assembling. The water content in natural granitoids (Fig. S1) were measured by
128 Fourier-transformation infrared (FT-IR) spectroscopy before and after thermal
129 property measurement (for details see Appendix A in Supplementary Material). The
130 bulk water content in granitoids (Table 1) was estimated from the volume fraction and
131 water content of each constituent mineral.
132
133 **Thermal property measurements**
134 High-pressure experiments were carried out with a YJ-3000t multi-anvil apparatus
135 installed at the Institute of Geochemistry, Chinese Academy of Sciences (IGCAS). A

pyrophyllite cube and a graphite sleeve were used as the pressure-transmitting medium and heater, respectively (Fig. 2a). High pressure was generated by six first-stage cubic tungsten carbide anvils. Prior to the high-pressure experiments, the pyrophyllite cube and other parts were pre-heated at 1173 K to remove absorbed water. Samples were isolated with a graphite heater using an alumina sleeve, which also served as a heat insulator to effectively restrict lateral heat flow. The pressure was calibrated via the phase transition of Bi (2.54 GPa at room temperature) and melting of halide (high temperature). It is known that pressure may drop by heating to some degree; however, slight pressure drop mainly occurs along cooling path above 1100 K from our experience of *in situ* X-ray diffraction (Yamazaki et al. 2012). The temperature was increased to 988 K in the present study, thus the error of pressure estimation is around 0.1 GPa. The temperature is calibrated with a K-type (NiCr-NiAl) thermocouple. The uncertainty in temperature measurement is less than ±0.5 °C.

Both thermal diffusivity and thermal conductivity were simultaneously measured at 0.3–1.5 GPa and 283 K–988 K using the transient plane-source method (Dzhavadov 1975; Osako et al. 2004). Fig. 2b shows the basic principles and instruments during thermal transport property measurement. Briefly, three double-polished samples of the same thickness were piled at the center of the pressure medium. An impulse heater with a diameter of 6.0 mm was placed on one interface between two disks, and a K-type thermocouple junction was set on the opposite interface. The samples were compressed in a stepwise fashion with a press load, heated to the desired temperature (283–988 K), and then cooled to the lowest

158 temperature setting with a rate of 10 °C/min. The temperature was changed in 50 or
159 100 K steps, and the thermal disturbance caused by impulse heating was monitored
160 using the thermocouple at each temperature step. At least three repeated
161 measurements for each temperature were performed to check the reproducibility.

162 A DC power supply controlled by an electronic switch, and providing
163 instantaneous pulse currents (~60 ms) initiated a thermal disturbance within the
164 samples. Transient heat flow caused by impulse heating passed through the sample
165 disk, and the corresponding transient signal was observed by the thermocouple as a
166 hump on the emf of the ambient temperature. MgO blocks in contact with the sample
167 served as heat sinks, which maintained a constant-temperature boundary condition.
168 After the experiments, the recovered samples were carefully examined under a
169 microscope to evaluate destruction or deformation. None was found. This result
170 suggests that the geometric deformation of samples during the experiments has little
171 influence on the experimental results.

172

173 **Data analysis**

174 Using the experimental setup (Fig. 2) and heat conduction theory, the
175 temperature variation, ΔT, at the position of the thermocouple can be expressed as
176 follows (Dzhavadov 1975; Osako et al. 2004):

177 $$\Delta T = A\sum_{n=1}^{\infty}\frac{1}{n^2}\sin\frac{n\pi}{3}\sin\frac{n\pi d}{h}\exp -n^2Bt\left[\exp(n^2B\tau)-1\right]: t>\tau \qquad (1)$$

178 where τ is the duration (s) of impulse heating, d is the distance (m) between the
179 impulse heater and the thermocouple, and h is the total height of three sample discs

(m). The quantities A and B are defined as follows:

$$A = \frac{2Qh}{\pi^2 \kappa S}, \qquad B = \frac{\pi^2 D}{h^2} \tag{2}$$

where Q is the power (W) of the impulse heating, S is the area of the impulse heater (m^2), κ is the thermal conductivity ($Wm^{-1}K^{-1}$), and D is the thermal diffusivity (mm^2s^{-1}). Previous studies have shown that ΔT in Eq. (1) will converge rapidly with increasing n, and summation up to n = 10 yields accurate values (Osako et al. 2004; Yoneda et al. 2009).

Sources of experimental uncertainty

In the present experiments, the accuracy of measured thermal transport properties (D and κ) in granitoids are mainly influenced by temperature, pressure, sample geometry and experimental setup/or method. The temperature disturbance across the sample associated with the pulse heating is ~3 K with 10 W pulse power. Thus, the effect of temperature heterogeneity on measured results can be ignored in our assembly (Fig. 2). Sample dimensions during compression and heating was corrected according to the equation of state of granite (Anderson and Kanamori 1968) with the assumption of isotropic contraction of the rock sample. Change of the impulse heater area was calculated by the method proposed by Wang et al. (2014). As a result, the total experimental errors in Eq. (2) mainly derived from temperature and pressure gradient and sample geometry were estimated to be less than 7% in this study.

RESULTS

In the transient plane-source method, direct conversion from current-voltage signal to temperature tignal can be applied to achieve detailed information about D and κ simultaneously. Fig. 3a illustrates the original curves of the voltage of the impulse heater and changes in the response voltage of monzogranite under 0.5 GPa and 283 K after pulse heating was recorded using a storage oscilloscope in Channel 1 (CH1) and Channel 2 (CH2), respectively. Based on the recorded emf of the ambient temperature, the thermal disturbance (voltage–time curve) monitored using the thermocouple can be converted to temperature–time curves (Fig. 3b). Although the initial part of the temperature profile is disturbed by induction noise from the current of the impulse heater, it does not affect the measurements. Parameters A and B are determined through least-squares fitting of the converted temperature–time curves using Eq. (1) up to n = 15 (Fig. 3b). Once A and B are known, D and κ from Eq. (2) are calculated in combination with other parameters.

Figs. 4a and 4b respectively show a decreasing, concave-up relationship between thermal diffusivity (D) and thermal conduction (κ) and temperature for the granites at 0.5 GPa. At lower temperatures (< 500 K) the heat transfer in granitoids is dominated by phonons (lattice vibrations), which decreases with increasing temperature. At higher temperatures (> 600 K) almost constant or slight increase in thermal diffusivity and thermal conductivity is approximated according to a T^3 dependency due to the heat transfer by photons (ballistic radiation). The increase is more pronounced for the thermal diffusivity and thermal conductivity of

224 monzogranite, granodiorite and alkaline granite, suggesting radiative heat transfer
225 starts playing a role. Thus, the temperature dependence of the thermal diffusivity and
226 thermal conductivity of each sample in this study can be fitted using the following
227 empirical forms (Höfer and Schilling 2002; Ray et al. 2006):

228 $$D(T) = a_0 + a_1 / T + a_2 / T^2 + a_3 \times T^3 \quad (3)$$

229 $$\kappa(T) = b_0 + b_1 / T + b_2 / T^2 + b_3 \times T^3 \quad (4)$$

230 where T is the absolute temperature, and the coefficients a_0, a_1, a_2, b_0, b_1, and b_2
231 approximate the heat transfer by phonons, a_3 and b_3 are due to the radiative heat
232 contribution. Granites with different mineralogy have room-temperature D of
233 1.46–2.08 mm^2s^{-1} which decreases to a constant ~0.8 ± 0.1 mm^2s^{-1} (>700 K) with
234 increasing temperature. The room–temperature κ of granites are in the range of
235 3.00–4.24 $Wm^{-1}K^{-1}$ and, similar to their D, decrease to a constant of ~2.2 ± 0.2
236 $Wm^{-1}K^{-1}$ with increasing temperature (Supplementary Table 2). For granite samples
237 with relatively low (19-26 vol%) quartz content, the decrease in thermal
238 diffusivity/conductivity is less, equivalent to about 30%–60% of the
239 room-temperature value up to 500 K (Figs. 4a and 4b). Thereafter, these properties
240 remain roughly constant or slightly increase at temperature up to 950 K. The
241 four-parameter fit Eqs. (3-4) describe the temperature dependence of D and κ well
242 within the experimental uncertainties (Table 2).

243 Figs. 4c and 4d show the pressure dependence of D and κ measured at different
244 temperature. The thermal diffusivity and thermal conductivity of all samples increase
245 with increasing pressure, which is consistent with theoretical analysis based on

Debye's analogy that suggests that D or κ should increase with pressure for most Earth-based materials (Hofmeister 2007). Increases in both D and κ with pressure can be linearly fitted to the following empirical relations:

$$D(P) = D_0 + c \times P \quad (5)$$

$$\kappa(P) = \kappa_0 + d \times P \quad (6)$$

where the fitting coefficients D_0, c, κ_0, and d are given in Table 2. The calculated pressure coefficients (c and d) for D or κ at room temperature are in the range of 0.18–0.29 $mm^2\ s^{-1}\ GPa^{-1}$ and 0.22–0.56 $Wm^{-1}\ K^{-1}\ GPa^{-1}$, respectively. It is worth noting that the pressure dependence in Eqs. (5-6) is only an empirical relationship rather than a theoretical formula, which may merely work at lower pressures (Hofmeister 2007).

In order to further explore the effect of pressure on thermal transport properties of granitoids, two samples (monzogranite and granodiorite) were measured again at 0.5–1.5 GPa and 283–988 K. As shown in Fig. 5, the results of D and κ in the first and second measurements are basically the same at 0.5 GPa. However, the remeasured κ of monzogranite (Fig. 5b) is higher than that in the first measurement at elevated temperature, which may reflect the contribution of ballistic radiation. At each pressure, the temperature dependence of D and κ for monzogranite and granodiorite is similar to that observed at 0.5 GPa (Figs. 4a and 4b). With increasing pressure from 0.5 GPa to 1.5 GPa, an increase of 9–24% and 9–19% in D and κ at the same temperature was observed for monzogranite and granodiorite, respectively, within the whole examined temperature range. In addition, previous investigations observed a minimum in

thermal diffusivity at the temperature of the α-β phase transition of quartz and the thermal diffusivity of β-quartz is higher than that of α-quartz above 846 K (Höfer and Schilling 2002; Branlund and Hofmeister 2007, 2008). In the present experiments, it is hard to evaluate the effect of the α-β phase transition of quartz on the thermal properties of granitoids (Figs. 4-5) because of very limited data points below and above 846 K.

The experimental errors for D and κ are less than 7% (Supplementary Table 2). These mainly originate from the uncertainty of the sample dimensions under high P-T conditions, the least-squares fitting procedures, thermal contact resistance, radiative heat loss, and some other parameters in Eq. (2). The present experimental results of thermal diffusivity/conductivity determined during heating are in good agreement with those obtained from the cooling cycle (gray symbols in Figs. 4a and 4b for monzogranite and granodiorite samples). Such data reproducibility suggests that the transient plane source method employed in this study is reproductible. Although the thicknesses of monzogranite and granodiorite samples are different in the first and second measurements, no influence of sample length on D and κ is observed (Figs. 4-5 and Supplementary Table 2), which would be expected if radiative heat transfer contributed significantly (Höfer and Schilling 2002).

DISCUSSION

Comparison with previous data

Fig. 6 shows a comparison of our data on D and κ of granites with the previous

results. All of the results of D and κ decrease with increasing temperature (<600 K), and asymptotically approach a high-temperature limit. Durham et al. (1987) investigated the thermal diffusivity of Atikokan and Stripa granites (with 23–31 vol% quartz content) at 300–673 K and hydrostatic confining pressures of 0.1–200 MPa. These results are in good agreement with data in this study. Seipold (1992) measured the thermal diffusivity of granitic samples at high pressures (up to 500 MPa) and temperature (up to 923 K) using the Ångström method. He argued that grain size and quartz content have no significant influence on the temperature and pressure dependence of the thermal transport properties; however, contributions from heat transfer by radiation up to 973 K were not found. As illustrated in Fig. 6a, the thermal diffusivity reported by Seipold (1992) is lower than ours and that of other researchers (Durhum et al. 1987; Maqsood et al. 2004; Ray et al. 2006; Whittington et al. 2009).

The thermal diffusivity of granite samples reported by Whittington et al. (2009) shows a rapid reduction at low temperature (<600 K), results at higher temperature (>600 K) are lower than those in the present study and previous investigations (Durham et al. 1987; Ray et al. 2006). The small D in those experiments with laser flash analysis may be partially due to the unavoidable formation of thermally induced cracks that reduce the heat transfer performance of the samples at high temperature. Another possibility for this discrepancy is that the ballistic heat transports in previous works (Durham et al. 1987; Ray et al. 2006) and the present study are stronger than those in Whittington et al.'s experiments, which only increases with temperature. Remarkably, although D and κ of granites were simultaneously determined by

312 Maqsood et al. (2004) at 253–333 K at ambient pressure, their results indicated a
313 rapid decrease in D and κ of granites with increasing temperature. The data of these
314 investigators are inconsistent with all existing results (Fig. 6a and 6b). The reason for
315 inconsistency in their results is unknown.

316 At relatively low temperatures (<500 K), the thermal diffusivity of charnockites
317 (Σ alkali-feldspar + plagioclase = 51–82%; 0.5–35% quartz; 1–16% pyroxene) and
318 enderbites (Σ alkali-feldspar + plagioclase = 39–49%; 22–44% quartz; 5–23%
319 pyroxene; 0.2–9% garnet; 0–13% biotite) determined by Ray et al. (2006) is
320 comparable with those from the present study and Whittington et al. (2009), as well as
321 the thermal diffusivity of tonalite-trondhjemite-granodiorite (TTG) rocks reported by
322 Merriman et al. (2013) and the average crust model proposed by Whittington et al.
323 (2009). However, Ray et al.'s data in the high-temperature range (500–823 K) show
324 an upward trend with increasing temperature, and their absolute values are higher than
325 our and Whittington et al.'s findings. This discrepancy may be due to either the
326 contribution of radiative heat to the bulk D of charnockites, which results in
327 enlargement of enderbites at high temperatures, or relatively higher quartz content in
328 Ray et al.'s study compared with others. Another possibility is due to variations in the
329 experimental setups and measurement techniques, as mentioned by Ray et al. (2006).

330 To date, except for the present experiments and Seipold (1992), few studies have
331 simultaneously measured D and κ of granites under high temperature and pressure.
332 Birch and Clark (1940), as well as Merriman et al. (2013), only determined κ of
333 granites at 300–1273 K and atmospheric pressure. Zhao et al. (2016) reported thermal

conductivities of Beishan granitic rocks under axial compression stress up to 45 MPa and temperature only up to 423 K. In addition, some researchers (e.g., Whittington et al. 2009; Merriman et al. 2013) used an indirect method (thermal diffusivity measurements) to retrieve thermal conductivity κ by combination of the specific heat capacity and density. As shown in Fig. 6b, the present results of κ in granitoids at low temperature (< 700 K) are consistent with those obtained in previous studies (Birch and Clark 1940; Seipold 1992; Whittington et al. 2009; Merriman et al. 2013; Zhao et al. 2016), except for the results obtained by Maqsood et al. (2004). At higher temperature (> 700 K), the data obtained in this study at 0.5 GPa are higher than the "average crust" calculated by Whittington et al. (2009) and those determined by Merriman et al. (2013) at atmospheric pressure. This difference may be caused by the enhancement of thermal conductivity by pressure in the present experiment compared to atmospheric pressure cases.

Factors influencing thermal transport properties

The thermal transport properties of rocks and minerals are affected by numerous factors, of which the most important are temperature, pressure, porosity, dominant mineral phase and mineralogical composition, water, grain boundary and anisotropy. Several of these factors are discussed briefly.

Temperature – Thermal diffusivity and thermal conductivity are functions of temperature. At a low temperature range (usually less than 700 K), heat transfer in crustal rocks is mainly caused by phonon conduction (lattice vibration), which is

356 inversely proportional to temperature, as shown in Figs. 4-6. This is because the
357 thermal contact resistance between mineral grains increases with the increase of
358 temperature due to thermal cracking, which causes the observed decrease in D/κ with
359 temperature (Clauser and Huenges 1995). At high temperatures (> 700 K), heat
360 radiation (photons) begins to contribute sizably to the overall heat transfer in most
361 polycrystalline materials. Radiative contributions to κ increase with the cube of
362 temperature (Clauser and Huenges 1995; Hofmeister 1999; Clauser 2009). This
363 phenomenon has been observed in mafic granulites by Ray et al. (2006) and in this
364 study, especially for monzogranite and granodiorite with relatively high plagioclase
365 contents. However, precisely evaluating the contribution of radiative heat to bulk
366 thermal properties under high-pressure experimental condition or in the Earth's
367 interior is difficult. This is because the radiative heat of most minerals and rocks in
368 the Earth's interior is unknown due to technical difficulties in measuring thermal
369 radiation under high pressure.

370 ***Pressure*** – Clauser and Huenges (1995) and Clauser (2006) revealed that the
371 effect of overburden pressure on thermal conductivity and thermal diffusivity is
372 twofold. Initially, fractures and microcracks (developed during stress release when
373 samples are brought to the surface) begin to close with increasing pressure. This
374 phenomenon reduces the thermal contact resistance and porosity. When an
375 overburden pressure of about 15 MPa is reached, this process comes to an end. If
376 pressure is increased further (> 40 MPa), a second process comes into effect, and
377 reductions in intrinsic porosity, i.e., voids which are not created by stress release, are

observed. The granite rock data (Figs. 4c and 4d) indicate a corresponding increase in κ in the order of 10% when the pressure exceeds 50 MPa (Clauser and Huenges 1995; Clauser 2006). Nevertheless, this effect gradually decreases with increasing temperature.

Modal mineralogy – Mineral proportions play an important role in thermal transport properties of low-porosity crystalline rocks. Crystalline rocks, such as granite, are mainly composed of quartz, and two feldspars with minor accessory minerals, including pyroxene, amphibole, muscovite and biotite, and the modes of these three minerals determines a rock's thermal conductivity/diffusivity (Clauser and Huenges 1995). Previous studies have shown that quartz has the highest thermal diffusivity (average D_{quartz} = 4.7 mm^2s^{-1}) at room temperature among the major minerals of the investigated rocks (Branlund and Hofmeister 2007). Feldspars contribute less, owing to their low thermal diffusivity of usually < 1 mm^2s^{-1} (Pertermann et al. 2008). Therefore, the thermal conductivity/diffusivity of crystalline rocks (especially of granite) are primarily determined by the amount of quartz in the sample.

Our results on D (Fig. 7a) and κ (Fig. 7b) of granites at 0.5 GPa and different temperatures show a positive linear dependence on quartz content, whereas a negative linear dependence on plagioclase content is observed in Figs. 7c and 7d. This observation is similar to those reported in Atikokan and Stripa granites (Durham et al. 1987), mafic granulites (Ray et al. 2006), and Beishan granitic rocks (Zhao et al. 2016).

To better understand the influence of mineral abundances on the bulk thermal properties of rocks, various mixing models for n-phase systems, such as the geometric mean (Lichtenecker 1924) and the Hashin–Shtrikman upper bound (Hashin and Shtrikman 1962), have been proposed to calculate D and κ of granites under the corresponding experimental conditions of temperature and pressure. Comprehensive overviews and case studies on such mixing models can be found in other studies (e.g., Clauser and Huenges 1995; Clauser 2009; Fuchs et al. 2013; Zhao et al. 2016). By combination of thermal properties (D and κ) of terminal minerals reported previously (Clauser and Huenges 1995; Hofmeister and Branlund 2007) and the volume fraction of each mineral observed in the present study (Table 1), the different mixing models were used to predict the thermal transport properties of granites. Fig. 8 compares the measured and calculated D and κ for two different models. As illustrated in Figs. 8a–8b, both the geometric mean and Hashin–Shtrikman upper bound show a reasonably good fit for predicting D and κ of our four granite samples, whereas these two models give rise to considerably larger uncertainties on calculated κ (Figs. 8c–8d). Remarkably, most of the evaluated mixing models used in previous studies (e.g., Fuchs et al. 2013, 2018; Zhao et al. 2016) also underestimated the thermal conductivity of the rocks. The reasons for the observed discrepancies between measured and calculated κ are numerous. Analytical and measurement errors, however, appear only being of secondary importance. These differences may as well result some extent from the physical-mathematical formulations of the evaluated mixing models, which describe in a rather simple manner the real, likely more complicated

422 nature of a rock. Both the geometric mean and Hashin–Shtrikman upper bound
423 models represent a layered structure of phases, and it is assumed that the
424 non-systematic (chaotic) arrangement of the mineral grains will lead to heat transfer
425 through isotropic rocks in a certain way. In anisotropic medium, the phenomenon of
426 vertical plane boundary is considerably retarded due to countless heat-refraction
427 events (Fuchs et al. 2018). Furthermore, the most crucial parameter is the uncertainty
428 in the knowledge of mineral thermal conductivity (in particular quartz, feldspar,
429 amphibole and pyroxenes in our suite of samples). Likewise, these minerals display
430 some thermal conductivity anisotropy in rock, which is also reflected in laboratory
431 measurements of rock samples. Our measured D and κ were obtained at high pressure
432 in this study, while available thermal transport properties for these rock forming
433 minerals were reported at atmospheric pressure in most cases (Clauser and Huenges
434 1995). The effect of water on our measured D and κ is another possibility. Future
435 work is demanded to resolve this discrepancy.

436 ***Water*** – Previous studies have demonstrated that hydration can significantly
437 reduce lattice thermal conductivity because protonation contributes structural disorder
438 to minerals and adds new vibrational modes (Hofmeister et al. 2006; Chang et al.
439 2017). In the present study, nearly the same water content (Table 1) obtained before
440 and after thermal conductivity measurement (0.02-0.10 wt.% H_2O) suggests that no
441 obvious dehydration occurs during the conductivity experiment. The bulk water
442 contents in granitoid samples are much lower than the loss on ignition
443 (Supplementary Table 1). In addition, no sharp jump in measured D and κ at high

444 temperatures were found in Figs 4 and 5. All of these observations suggest that the
445 effect of granitoid dehydration on our measured D and κ is negligible in this case.
446 However, quantitative effect of water content on thermal properties of granitoids
447 remains unknown, which needs to be investigated in future.

448 ***Grain boundary*** – It is well known that thermal resistance at grain boundaries
449 potentially affects heat transport in a polycrystalline material. The thermal resistance
450 (inverse of thermal conductivity) of a polycrystalline sample (κ_{poly}^{-1}) can be expressed
451 as (Smith et al. 2003): $\kappa_{poly}^{-1} = \kappa_{single}^{-1} + nR_{GB}$, where κ_{single}^{-1}, n and R_{GB} stand for the
452 thermal resistance of a single crystal, the number of grain boundaries per meter along
453 heat flow and grain boundary resistance, respectively. Based on microphotographs of
454 granitoid samples depicted in Fig.1, the average grain size in our sample is ~1 mm,
455 which indicates that n is on the order of 10^3. Combined with the experimental results
456 of single crystal κ on quartz (Branlund and Hofmeister 2007), plagioclase feldspar
457 (Branlund and Hofmeister 2012) and alkali feldspar (Pertermann et al. 2008), R_{GB} is
458 estimated to be approximately 1×10^{-6} m^2K/W and 1×10^{-8} m^2K/W, respectively, for
459 granodiorite and syenogranite at 0.5 GPa and 300 K. The value of R_{GB} for
460 syenogranite is comparable with that in ceramic Al_2O_3 at ambient conditions (R_{GB} ~1
461 $\times 10^{-8}$ m^2K/W) (Smith et al. 2003), but smaller than that in granodiorite with less
462 quartz. This estimate shows that the thermal resistance (R_{GB}) in granitoids decreases
463 with increasing quartz contents, thus implying an increase in the contribution of grain
464 boundary scattering to the bulk κ.

465 Apart from temperature, pressure, modal mineralogy, water and grain boundary,

466 thermal transport properties of a rock also vary with porosity and crack. For
467 crystalline granite, the effect of porosity on D and κ of natural granitoid should be tiny
468 due to their very small porosity (1%, Clauser and Huenges 1995; Clauser 2006, 2011).
469 It is expected that original pores and cracks (if present) derived from mineral grains
470 expanded anisotropically during heating should shrink and then porosity and crack
471 will approach zero with increasing pressure. Because rocks form under high confining
472 pressure, thermal cracking should not occur in Earth's crust. Consequently, porosity
473 will be minimal at high temperatures and high pressures. On the other hand,
474 dual-contact methods were applied to measure D and κ of granitoids in the present
475 experiments. The metal-silicate interface provides an additional resistance and reduce
476 heat transfer. The sample and thermocouple will expand differently during heating, as
477 well as opening of cracks, which probably creates additional contact losses
478 (Hofmeister 1999, 2007; Hofmeister and Branlund 2007). For these reasons,
479 laboratory measurements of D and κ may underestimate a rock's true heat transport
480 properties.

481

482 **Heat capacity**

483 The heat capacity of a rock can be determined by using the following equation:

484 $$C = \frac{\kappa}{\rho D} \qquad (7)$$

485 where C is the specific heat capacity and ρ is the density (Clauser and Huenges 1995;
486 Clauser 2011). The theoretical "bulk" heat capacity of granite was also calculated
487 from the previously reported specific heat capacities ($C_P(T)$) of end-member minerals

(Berman and Brown 1985; Clauser 2011) on the basis of the modal abundance of each mineral (listed in Table 1), i.e., $C_P(T) = \sum_i X_i C_{P,i}(T)$, where X_i is the volume fraction of the *i*-th mineral in granite (Supplementary Table 3). Fig. 9 shows the temperature dependence of the specific heat capacity of our four natural granite samples. The uncertainties related to the calculated specific heat capacity data points are about 10%. The heat capacities of granites determined from Eq. (7) in this study are consistent with the theoretically predicted "bulk" heat capacities within the limits of experimental error. This finding indicates that the simple mixing rule is suitable for determining the specific heat capacity of rocks within about 10%.

IMPLICATIONS

Seismic and magnetotelluric surveys occasionally reveal the ubiquitous presence of low-velocity and high-conductivity zones in the upper-to-middle crust in southern Tibet (e.g., Pham et al. 1986; Nelson et al. 1996; Brown et al. 1996; Wei et al. 2001; Li et al. 2003; Bai et al. 2010; Hacker et al. 2014). Several hypotheses have been proposed to account for these observations, including the presence of aqueous fluids (Nelson et al. 1996; Wei et al. 2001), graphite (Glover 1996), and partial melting (Li et al. 2003; Hacker et al. 2014). Among these models, partial melting, which strongly depends on temperature, is thought to be the best candidate to explain observations. Unfortunately, it is unclear if the crust in southern Tibet has a high enough temperature to produce partial melting. Surface heat flow data are of significant importance for the characterization of the thermal regime and to reveal the

geodynamic processes of continental lithosphere (Huppert and Sparks 1988; Bea 2012; Furlong and Chapman 2013), which depends more on the last tectonothermal activity and decay of unstable radioactive isotopes rather than on the age of the orogeny. Surface heat flow measurements have indicated that the heat flow in southern Tibet (> 80 mW/m^2) (Francheteau et al. 1984) is significantly higher than the mean heat flows of other continents (65 mW/m^2) (Pollack et al. 1993). In the lithosphere of the Earth, heat conduction or diffusion is the dominant transport process, except for settings where appreciable fluid flow or magmas segregated from anatectic zones provides a mechanism for heat advection. Numerical modeling by Huppert and Sparks (1988) indicated that heat advected by mafic magmas can produce crustal melts. Since the process is very fast it is not directly influenced by the heat production of the source.

The temperature distribution within the Earth largely depends on the thermal properties of major rocks, surface heat flow, heat conduction, and heat production of the relevant lithology. Establishing a detailed temperature profile of the crust is necessary to better understand the process of melting in southern Tibet. In this case, the finite element method was applied to solve the Fourier heat conduction in one dimension (for details see Appendix B in Supplementary Material). To simplify the model, the depth from the upper crust to the lower crust throughout southern Tibet was calculated, and heat conduction was considered as the only mechanism. A typical and moderate value of the surface heat flow (80 mW/m^2) in southern Tibet (Francheteau et al. 1984) was used in our calculation. The distribution of radiative heat production, both in the horizontal and vertical directions, is poorly constrained in

532 southern Tibet, and thus the constant values of 0.64, 1.21, and 1.65 μW/m^3 (Huppert
533 and Sparks 1988; Bea 2012; Furlong and Chapman 2013) were employed in this study
534 to roughly represent the low, middle, and high heat production areas of the upper to
535 lower crust, respectively. In this calculation, subcrustal heat flows at 60 km depth
536 were fixed at 50, 25, and 5 mW/m^2 according to the different radiative heat
537 production values applied to ensure that the surface heat flow is maintained at 80
538 mW/m^2. For comparison, the model with a constant κ of 3.0 Wm^{-1}K^{-1} was also
539 calculated, and the surface temperature was fixed to 283 K.

540 Fig. 10 shows a comparison of our calculated geotherms with the solidus curves
541 of muscovite and biotite dehydration (Patiño Douce and Harris 1998). The geotherms
542 calculated with radiative heat production values of 0.64, 1.21, and 1.65 μW/m^3
543 intersect with the dehydrated melting line of muscovite at ~19, ~24, and ~35 km,
544 respectively. This suggests that partial melting due to dehydration of hydrous minerals
545 can occur in such shallow crust. The corresponding melting temperature ranges are
546 945–1078 K. The depth of partial melting induced by biotite dehydration is about 5
547 km deeper than that of muscovite dehydration. These deeper depths are consistent
548 with those reported by geophysical observations. This observation supports the partial
549 melting model for anomalies in the crust of southern Tibet (Nelson et al. 1996). By
550 contrast, the geotherms derived from constant κ show a large gradient and do not
551 intersect with the dehydration curves within the depth range of 30 km. This difference
552 indicates that geothermal calculation with constant thermal properties obtained at
553 ambient conditions may underestimate both the temperature and geothermal gradient

within the crust (Merriman at al. 2013). On the other hand, numerical models indicate that partial melting will appear deeper in the crust than expected and would require a higher temperature (Fig. S2), if the surface heat flow is decreased to 60 mW/m^2 and the other parameters remain unchanged.

By definition, granite has a relatively high quartz content and, thus, relatively high κ. However, other main rocks with relative low quartz content in the upper crust have a lower κ than that of granitic rocks. Clearly, the low κ of minerals and rocks will further reduce the geothermal gradient, leading to a shallow intersecting depth of the geotherm with the dehydrated solidus. Thus, the present estimate may provide a lower limit to the possible depth of partial melting. In the future, a greater amount of experimental data on the thermal properties of relevant rocks are needed to further understand the physical states and thermal evolution within the Earth's crust.

ACKNOWLEDGMENTS

We thank associate editor (S. Demouchy), Bruno Scaillet and one anonymous reviewer for their constructive comments that greatly improved the manuscript. We also appreciate the helps of Prof. Hongfeng Tang for thin section identification, Prof. Xiaozhi Yang for FTIR measurements and Prof. Yoneda for assistance in data fitting. This study was supported by the Strategic Priority Research Program (B) of the Chinese Academy of Sciences (XDB18010401), the 1000Plan Program for Young Talents and Hundred Talent Program of CAS, NSF of China (41773056, 41303048) and Science Foundation of Guizhou Province (2017-1196, 2018-1176).

The authors declare no competing financial interests.

REFERENCES CITED

Abdulagatov, Z.Z., Abdulagatova, I.M., and Emirov, S.N. (2009) Effect of temperature and pressure on the thermal conductivity of sandstone. International Journal of Rock Mechanics and Mining Sciences, 46, 1055–1071.

Anderson, D.L., and Kanamori, H. (1968) Shock-wave equations of state for rocks and minerals. Journal of Geophysical Research,73(20), 6477–6502.

Annen, C., Blundy, J.D., and Sparks, R.S.J. (2005) The genesis of intermediate and silicic magmas in deep crustal hot zones. Journal of. Petrology, 47, 505–539.

Bai, D., Unsworth, M.J., Meju, M.A., Ma, X., Teng, J., Kong, X., Sun, Y., Sun, J., Wang, L., Jiang, C., Zhao, C., Xiao, P., and Liu, M. (2010) Crustal deformation of the eastern Tibetan plateau revealed by magnetotelluric imaging. Nature geoscience, 3(5), 358–362.

Bea, F. (2012) The sources of energy for crustal melting and the geochemistry of heat-producing elements. Lithos, 153, 278–291.

Berman, R.G., and Brown, T.H. (1985) Heat capacity of minerals in the system Na_2O-K_2O-CaO-MgO-FeO-Fe_2O_3-Al_2O_3-SiO_2-TiO_2-H_2O-CO_2: representation, estimation, and high temperature extrapolation. Contributions to Mineralogy and Petrology, 89(2-3), 168–183.

Birch, A.F., and Clark, H. (1940) The thermal conductivity of rocks and its dependence upon temperature and composition. American. Journal of Science, 238,

529–558.

Branlund, J.M., Kameyama, M.C., Yuen, D.A., and Kaneda, Y. (2000) Effects of temperature-dependent thermal diffusivity on shear instability in a viscoelastic zone: implications for faster ductile faulting and earthquakes in the spinel stability field. Earth and Planetary Science Letters, 182(2), 171–185.

Branlund, J.M., and Hofmeister, A.M. (2007) Thermal diffusivity of quartz to 1000 ºC: effects of impurities and the α-β phase transition. Physics and Chemistry of Minerals, 34(8), 581–595.

Branlund, J.M., and Hofmeister, A.M. (2008) Factors affecting heat transfer in natural SiO_2 solids. American Mineralogist, 93(10), 1620–1629.

Branlund, J.M., and Hofmeister, A.M. (2012) Heat transfer in plagioclase feldspars. American Mineralogist, 97(7), 1145–1154.

Chang, Y.Y., Hsieh, W.P., Tan, E., and Chen, J. (2017) Hydration-reduced lattice thermal conductivity of olivine in Earth's upper mantle. Proceedings of the National Academy of Sciences, 114(16), 4078–4081.

Clark, C., Fitzsimons, I.C.W., Healy, D., and Harley, S.L. (2011) How does the continental crust get really hot? Elements, 7, 235–240.

Clauser, C. (2006) Geothermal energy. Landolt-Börnstein, group VIII: advanced materials and technologies, 3, 493–604.

Clauser, C. (2009) Heat transport processes in the Earth's crust. Surveys in Geophysics, 30(3), 163–191.

Clauser, C. (2011) Thermal storage and transport properties of rocks, I: Heat capacity

620 and latent heat. In Encyclopedia of solid earth geophysics (pp. 1423–1431).
621 Springer, Dordrecht.
622 Clauser, C., and Huenges, E. (1995) Thermal conductivity of rocks and minerals.
623 Rock physics & phase relations, 3, 105–126.
624 Durham, W.B., Mirkovich, V.V., and Heard, H.C. (1987) Thermal diffusivity of
625 igneous rocks at elevated pressure and temperature. Journal of Geophysical
626 Research, 92, 11615–11634.
627 Dzhavadov, L.N. (1975) Measurement of thermophysical properties of dielectrics
628 under pressure. High Temperatures – High Pressures., 7, 49–54.
629 Francheteau, J., Jaupart, C., Shen, X.J., Kang, W.H., Lee, D.L., Bai, J.C.., Wei, H.P.,
630 Deng, H.Y. (1984). High heat flow in southern Tibet. Nature, 307(5946), 32–36.
631 Fuchs, S., Schütz, F., Förster, H.J., and Förster, A. (2013) Evaluation of common
632 mixing models for calculating bulk thermal conductivity of sedimentary rocks:
633 correction charts and new conversion equations. Geothermics, 47, 40–52.
634 Fuchs, S., Förster, H.J., Braune, K., and Förster, A. (2018) Calculation of thermal
635 conductivity of low‐porous, isotropic plutonic rocks of the crust at ambient
636 conditions from modal mineralogy and porosity: A viable alternative for direct
637 measurement? Journal of Geophysical Research, 123(10), 8602–8614.
638 Furlong, K.P., and Chapman, D.S. (2013) Heat flow, heat generation, and the thermal
639 state of the lithosphere. Annual Review of Earth and Planetary Sciences, 41,
640 385–410.
641 Glover, P.W.J. (1996) Graphite and electrical conductivity in the lower continental

642 crust: a review. Physics and Chemistry of the Earth, 21, 279–287.
643 Hacker, B.R., Ritzwoller, M.H., and Xie, J. (2014) Partially melted, mica-bearing
644 crust in Central Tibet. Tectonics, 33(7), 1408–1424.
645 Hashin, Z., and Shtrikman, S. (1962) A variational approach to the theory of the
646 effective magnetic permeability of multiphase materials. Journal of Applied
647 Physics, 33, 3125–3131.
648 Hemingway, B.S., and Robie, R.A. (1990) Heat capacities and thermodynamic
649 properties of annite (aluminous iron biotite). American Mineralogist, 75(1-2),
650 183–187.
651 Höfer, M., and Schilling, F.R. (2002) Heat transfer in quartz, orthoclase, and sanidine
652 at elevated temperature. Physics and Chemistry of the Earth, 29(9), 571–584.
653 Hofmeister, A. M. (1999) Mantle values of thermal conductivity and the geotherm
654 from phonon lifetimes. Science, 283, 1699–1706.
655 Hofmeister, A.M. (2007) Pressure dependence of thermal transport properties.
656 Proceedings of the National Academy of Sciences, 104, 9192–9197
657 Hofmeister, A.M., Pertermann, M., Branlund, J.M., and Whittington, A.G. (2006)
658 Geophysical implications of reduction in thermal conductivity due to hydration.
659 Geophysical Research Letters, 33(11), L11310.
660 Huppert, H.E., and Sparks, R.S.J. (1988) The generation of granitic magmas by
661 intrusion of basalt into continental crust. Journal of Petrology, 29, 599–624.
662 Kanamori, H., Fujii, N., and Mizutani, H. (1968) Thermal diffusivity measurement of
663 rock-forming minerals from 300° to 1100° K. Journal of Geophysical Research,

73(2), 595–605.

Lichtenecker, K.V. (1924) Der elektrische Leitungswiderstand künstlicher und natürlicher Aggregate. Phys. Z, 25(10), 225–233.

Li, S., Unsworth, M.J., Booker, J.R., Wei, W., Tan, H., and Jones, A.G. (2003) Partial melt or aqueous fluid in the mid-crust of Southern Tibet? Constraints from INDEPTH magnetotelluric data. Geophysical Journal International, 153, 289–304.

Maqsood, A., Gul, I.H., and Anisur Rehman, M. (2004) Thermal transport properties of granites in the temperature range 253–333 K. Journal of Physics D: Applied Physics, 37(9), 1405–1409.

McKenzie, D., Jackson, J., and Priestley, K. (2005) Thermal structure of oceanic and continental lithosphere. Earth and Planetary Science Letters, 233(3-4), 337–349.

Merriman, J.D., Whittington, A.G., Hofmeister, A.M., Nabelek, P.I., and Benn, K. (2013) Thermal transport properties of major Archean rock types to high temperature and implications for cratonic geotherms. Precambrian Research, 233, 358–372.

Miao, S., Li, H., and Chen, G. (2014) The temperature dependence of thermal conductivity for lherzolites from the North China Craton and the associated constraints on the thermodynamic thickness of the lithosphere. Geophysical Journal International, 197(2), 900–909.

Nabelek, P.I., Whittington, A.G., and Hofmeister, A.M. (2010) Strain heating as a mechanism for partial melting and ultrahigh temperature metamorphism in convergent orogens: Implications of temperature dependent thermal diffusivity and

686 rheology. Journal of Geophysical Research, 115(B12), B12417.
687 Nelson, K.D., Zhao, W., Brown, L.D., Kuo, J., Che, J., Liu, X., Klemperer S.L.,
688 Makovsky, Y., Meissner, R., Mechie, J., Kind, R., Wenzel, F., Ni, J., Nabelek, J.,
689 Leshou, C., Tan, H., Wei, W., Jones, A.G., Booker, J., Unsworth, M., Kidd, W.,
690 Hauck, M., Alsdorf, D., Ross, A., Cogan, M., Wu, C., Sandvol, W., and Edwards, M.
691 (1996) Partially molten middle crust beneath southern Tibet: synthesis of project
692 INDEPTH results. Science, 274, 1684–1688.
693 Osako, M., Ito, E., and Yoneda, A. (2004) Simultaneous measurements of thermal
694 conductivity and thermal diffusivity for garnet and olivine under high pressure.
695 Physics of the Earth and Planetary Interiors, 143, 311–320.
696 Paterson, M.S. (1982) The determination of hydroxyl by infrared absorption in quartz,
697 silicate glasses and similar materials. Bulletin de Mineralogie, 105, 20–29.
698 Patiño Douce, A.E., and Harris, N. (1998) Experimental constraints on Himalayan
699 anatexis. Journal of Petrology, 39, 689–710.
700 Pertermann, M., Whittington, A.G., Hofmeister, A.M., Spera, F.J., and Zayak, J. (2008)
701 Transport properties of low-sanidine single-crystals, glasses and melts at high
702 temperature. Contributions to Mineralogy and Petrology, 155(6), 689–702.
703 Pham, V.N., Boyer, D., Therme, P., Yuan, X.C., Li, L., and Jin, G.Y. (1986). Partial
704 melting zones in the crust in southern Tibet from magnetotelluric results. Nature,
705 319(6051), 310–314.
706 Pollack, H.N., and Chapman, D.S. (1977) On the regional variation of heat flow,
707 geotherms, and lithospheric thickness. Tectonophysics, 38, 279–296

Pollack, H.N., Hurter, S.J., and Johnson, J.R. (1993) Heat flow from the Earth's interior: analysis of the global data set. Review of Geophysics, 31, 267–280.

Ray, L., Förster, H.J., Schilling, F.R., Förster, A. (2006) Thermal diffusivity of felsic to mafic granulites at elevated temperatures. Earth and Planetary Science Letters, 251, 241–253.

Sawyer, E.W., Cesare, B., and Brown, M. (2011) When the continental crust melts. Elements, 7, 229–234.

Seipold, U. (1992) Depth dependence of thermal transport properties for typical crustal rocks. Physics of the Earth and Planetary Interiors, 69(3-4), 299–303.

Smith, D.S., Fayette, S., Grandjean, S., Martin, C., Telle, R., and Tonnessen, T. (2003) Thermal resistance of grain boundaries in alumina ceramics and refractories. Journal of the American Ceramic Society, 86(1), 105–111.

Wang, C., Yoneda, A., Osako, M., Ito, E., Yoshino, T., and Jin, Z. (2014) Measurement of thermal conductivity of omphacite, jadeite, and diopside up to 14 GPa and 1000 K: Implication for the role of eclogite in subduction slab. Journal of Geophysical Research, 119(8), 6277–6287.

Wei, W., Unsworth, M., Jones, A., Booker, J., Tan, H., Nelson, D., Chen, L., Li, S., Solon, K., Bedrosian, P., Jin, S., Deng, M., Ledo, J., Kay, D., and Robert, B. (2001) Detection of widespread fluids in the Tibetan crust by magnetotelluric studies. Science, 292, 716–718.

Whittington, A.G., Hofmeister, A.M., and Nabelek, P.I. (2009) Temperature-dependent thermal diffusivity of the Earth's crust and implications for

730 magmatism. Nature, 458, 319–321.

731 Yamazaki, D., Ito, E., Yoshino, T., Yoneda, A., Guo, X., Zhang, B., Sun, W.,
732 Shimojuku, A., Tsujino, N., Kunimoto, T., Higo, Y., and Funakoshi, K. (2012)
733 P-V-T equation of state for ε-iron up to 80 GPa and 1900 K using the Kawai-type
734 high pressure apparatus equipped with sintered diamond anvils. Geophysical
735 Research Letters, 39(20), L20308, doi:10.1029/2012GL053540.

736 Yoneda, A., Osako, M., and Ito, E. (2009) Heat capacity measurement under high
737 pressure: A finite element method assessment. Physics of the Earth and Planetary
738 Interiors, 174(1–4), 309–314.

739 Zhao, X.G., Wang, J., Chen, F., Li, P.F., Ma, L.K., Xie, J.L., and Liu, Y.M. (2016)
740 Experimental investigations on the thermal conductivity characteristics of Beishan
741 granitic rocks for China's HLW disposal. Tectonophysics, 683, 124–137.

742

743

744 **Figure captions**

745 **Fig. 1** Microphotographs of granitoid samples, under XPL, used in this study. (a)
746 Granodiorite, (b) Syenogranite, (c) Monzogranite, (d) Alkaline granite. Qtz = quartz;
747 Alk fsp = Alkali-feldspar; Pl = plagioclase; Bt = biotite; Amp = amphibole (Refer to
748 Tables 1 and 2 for additional information).

749

750 **Fig. 2** (a) Schematic cross section of the sample assembly for thermal properties
751 measurements, (b) Schematic diagram of transient plane source method.

752

753 **Fig. 3** (a) An example of the oscilloscope display for monzogranite sample under
754 0.5 GPa and room temperature in the present study. Channels 1 and 2 were used to
755 monitor voltage for impulse heater (Fig. 2a) and thermocouple output, respectively.
756 Channel 2 data were magnified 1000 times by a DC amplifier. (b) A typical example
757 showing the corresponding temperature-time curve (which was converted from the
758 digitized data of voltage-time curve for thermocouple output as indicated by dotted
759 rectangle in (a)) were used for data fitting to determine parameters A and B in Eq. (2).

760

761 **Fig. 4** Effects of temperature and pressure on thermal properties of granitoids.
762 Temperature dependence of D (a) and κ (b) at 0.5 GPa; pressure dependence of D (c)
763 and κ (d) at temperature of 300, 600 and 900 K. The gray squares (syenogranite) and
764 diamonds (granodiorite) in a and b were measured during cooling. The open circles
765 and diamonds in c and d represent the data were remeasured for monzogranite and
766 granodiorite at 0.5-1.5 GPa and 283-988 K. The grey shadow areas in c and d show
767 the pressure dependence at room temperature (300 K).

768

769 **Fig. 5** Second measurements of temperature dependence of D and κ for
770 monzogranite (a and b) and granodiorite (c and d), respectively, at a pressure of 0.5,
771 1.0 and 1.5 GPa. Open squares and circles represent the first measurements of D and κ
772 for monzogranite and granodiorite at 0.5 GPa.

773

774 **Fig. 6** Comparison of D (a) and κ (b) of granites at 0.5 GPa (red solid lines)
775 obtained in the present study with previous experimental data. All previous
776 experiments were performed at atmospheric pressure, except for Durham et al. (1987)
777 up to 200 MPa and Seipold (1992) up to 500 MPa. Thermal diffusivity and thermal
778 conductivity for average crust were calculated by Whittington et al. (2009).

779

780 **Fig. 7** Influence of quartz and plagioclase contents on D (a) and κ (b) of granitoids
781 at 0.5 GPa and three different temperatures.

782

783 **Fig. 8** Comparison between measured and modeled thermal properties in
784 granodiorite, syenogranite, monzogranite and alkaline granite. D calculated from
785 geometric mean (a), and Hashin-Shtrikman upper bound (b); κ calculated from
786 geometric mean (c), and Hashin-Shtrikman upper bound (d).

787

788 **Fig. 9** Temperature dependence of specific heat capacity for four granites samples
789 under 0.5 GPa. Data points were calculated from the present measured D and κ in Eq.
790 (7). Solid red lines represent theoretical "bulk" heat capacity of granite, which were
791 determined from previous reported specific heat capacity ($C_P(T)$) of end-member
792 minerals (Berman and Brown 1985; Clauser 2011) using the relation
793 $C_P(T) = \sum_i X_i C_{P,i}(T)$ and modal abundance of each mineral (Table 1).

794

795 **Fig. 10** Comparison of geotherms modeled for granitic upper-middle crust with

796 solidus curves of muscovite and biotite dehydration (Patiño Douce and Harris 1998).
797 Black dashed lines and dark cyan solid lines represent geotherms calculated from a
798 constant κ ~3.5 $Wm^{-1}K^{-1}$ and a κ as a function of temperature and pressure,
799 respectively. Numbers represent different radiative heat production in $\mu W/m^3$. The
800 heat flux is fixed at 80 mW/m^2 for all models.

Table 1 Geological description of natural granitoids.

			Mineral modes (in vol%)						Water content (wt.%)	
Sample name	Rock type	Description of rock samples	Pl	Alk fsp	Qtz	Bt	Amp	Density (kg/m^3)	Before†	After‡
DL-1	Granodiorite	Dark gray, medium-to-coarse grained texture, amphibole is slightly altered	52 (3)	16 (2)	19 (2)	5 (1)	8 (1)	2.760×10^3	0.096 (12)	0.091 (11)
GCH-1	Monzogranite	Light grey, fresh and non-altered biotite, medium grained texture	35 (2)	31 (2)	26 (2)	7 (1)	1 (1)	2.705×10^3	0.061 (9)	0.062 (10)
GCH-2	Syenogranite	Gray white, fresh no alteration, coarse-grained texture	26 (2)	42 (2)	29 (2)	3 (1)	-	2.658×10^3	0.042 (7)	0.040 (8)
TLP-1	Alkaline granite	Milky white, fresh no alteration, fine-to-medium grained texture	6 (1)	60 (4)	32 (3)	2 (1)	-	2.733×10^3	0.023 (5)	0.024 (6)

Pl = plagioclase; Alk fsp = alkali-feldspar; Qtz = quartz; Bt = biotite; Amp = amphibole.

† and ‡ denote the water content before and after the thermal conductivity measurements.

Table 2 Coefficients of fitting parameters for thermal diffusivity (D) and thermal conductivity (κ) as functions of temperature and pressure.

	$D(T) = a_0 + a_1/T + a_2/T^2 + a_3 \times T^3$ at 0.5 GPa					$D(P) = D_0 + cP$ at 300 K		
	a_0 ($mm^2\ s^{-1}$)	a_1 ($mm^2\ s^{-1}\bullet\ K$)	a_2 ($mm^2\ s^{-1}\bullet\ K^2$)	a_3 ($mm^2\ s^{-1}\bullet\ K^{-3}$)	R^2	D_0 ($mm^2\ s^{-1}$)	c ($mm^2\ s^{-1}\ GPa^{-1}$)	R^2
Syenogranite	0.595 (498)	37.770 (372)	109988 (68510)	-5.827 (2.672)E-11	0.994	1.952 (32)	0.223 (47)	0.957
Alkaline granite	0.928 (251)	-89.393 (178)	106029 (31709)	-1.619 (1.475)E-10	0.998	1.799	0.290	–
Monzogranite	0.550 (417)	87.459 (302)	62517 (54793)	-3.904 (2.465)E-12	0.993	1.528 (19)	0.238 (24)	0.995
Monzogranite *	0.601 (96)	88.252 (73)	61586 (13885)	-2.538 (4.506)E-11	0.998	1.499 (38)§	0.310 (41)§	0.935§
Monzogranite **	0.410 (143)	253.450 (107)	43139 (20116)	9.395 (6.825)E-11	0.997	0.835 (19)†	0.147 (18)†	0.993†
Monzogranite ***	0.121 (263)	551.142 (199)	-7641 (3719)	1.971 (1.267)E-10	0.992	0.701 (9)‡	0.111 (8)‡	0.999‡
Granodiorite	1.135 (147)	-369.143 (108)	131298 (19870)	-2.241 (0.747)E-10	0996	1.353 (35)	0.180 (52)	0.961
Granodiorite*	0.521 (88)	122.327 (66)	38752 (12483)	4.689 (4.397)E-11	0.997	1.289 (35)§	0.301 (39)§	0.919§
Granodiorite**	0.627 (57)	56.719 (43)	60452 (8152)	-1.868 (2.871)E-11	0.999	0.748 (18)†	0.139 (16)†	0.993†
Granodiorite***	0.424 (103)	231.752 (78)	42814 (14637)	8.151 (5.155)E-11	0.998	0720 (2)‡	0.036 (2)‡	0.998‡
	$\kappa(T) = b_0 + b_1/T + b_2/T^2 + b_3 \times T^3$ at 0.5 GPa					$\kappa(P) = \kappa_0 + dP$ at 300 K		
	b_0 ($Wm^{-1}\ K^{-1}$)	b_1 (Wm^{-1})	b_2 ($Wm^{-1}\bullet K$)	b_3 (($Wm^{-1}\bullet K^2$)	R^2	κ_0 ($Wm^{-1}\ K^{-1}$)	d ($Wm^{-1}\ K^{-1}\ GPa^{-1}$)	R^2
Syenogranite	1.576 (741)	563 (553)	53451 (10180)	4.242 (3.971)E-011	0.994	4.116 (29)	0.219 (45)	0.959
Alkaline granite	3.860 (296)	-1129 (211)	327492 (37482)	-7.249 (1.744)E-10	0.999	3.657	0.558	–
Monzogranite	1.280 (213)	583 (155)	1874 (2805)	4.346 (1.262)E-10	0.999	3.137 (105)	0.434 (135)	0.955
Monzogranite *	1.886 (318)	429 (244)	805 (460)	9.622 (1.495)E-11	0.987	3.069 (79)§	0.589 (84)§	0.924§
Monzogranite **	1.957 (159)	424 (120)	19906 (2237)	1.206 (0759)E-10	0.997	2.473 (8)†	0.308 (7)†	0.999†
Monzogranite ***	1.919 (276)	584 (209)	-401 (390)	1.916 (1.331)E-10	0.995	2.295 (12)‡	0.273 (11)‡	0.999‡
Granodiorite	3.595 (349)	-1356 (257)	335774 (47088)	-4.470 (1.770)E-10	0.980	2.721 (73)	0.482 (109)	0.975
Granodiorite*	2.373 (199)	-445 (151)	171587 (28270)	-6.420 (9.958)E-11	0.991	2.688 (32)§	0.545 (35)§	0.984§
Granodiorite**	1.700 (270)	89 (204)	99221 (38324)	2.264 (1.350)E-10	0.991	2.026 (24)†	0.177 (22)†	0.992†
Granodiorite***	1.169 (487)	584 (369)	23957 (69113)	5.068 (2.434)E-10	0978	1.923 (44)‡	0.200 (41)‡	0.980‡

*, ** and *** represent that the thermal properties of monzogranite and granodiorite were remeasured under 0.5, 1.0 and 1.5 GPa, respectively, with various temperature (283-988 K).
§Parameters were obtained by simultaneous fitting the results from the first and second measurements at 0.5 GPa.
† and ‡ denote that the parameters of monzogranite and granodiorite were calculated from the second measurements at 600 K and 900 K (shown in Figs. 4c and 4d), respectively, with different pressure (0.5, 1.0 and 1.5 GPa).

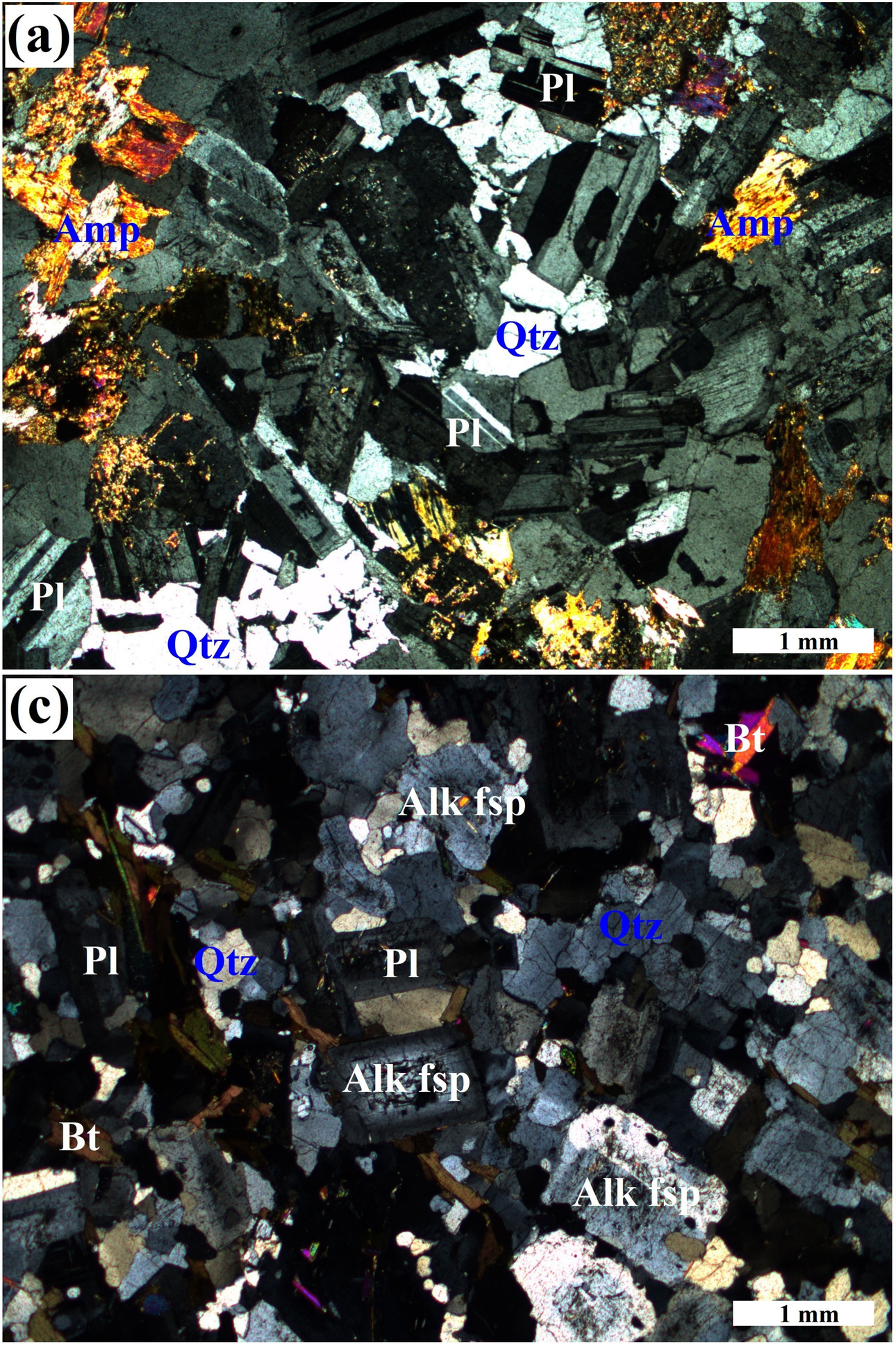
(a)
Pl
Amp
Amp
Qtz
Pl
Pl
Qtz
1 mm
(b)
Qtz
Alk fsp
Pl
Alk fsp
Qtz
Qtz
Pl
Qtz
1 mm
(c)
Bt
Alk fsp
Qtz
Pl
Qtz
Pl
Alk fsp
Bt
Alk fsp
1 mm
(d)
Alk fsp
Alk fsp
Qtz
Alk fsp
Qtz
Qtz
1 mm

Fig. 1

(a)

Pyrophyllite

MgO

Graphite heater

Sample

Al_2O_3

Impulse heater

Thermocouple

Cu Coil

10 mm

Impulse heater

Thermocouple

(b)

Thermocouple

Sample

Planar source

emf of thermocouple

DC Amplifier

Control Switch

DC Power Supply

Storage Oscilloscope

CH1 CH2

Fig. 2

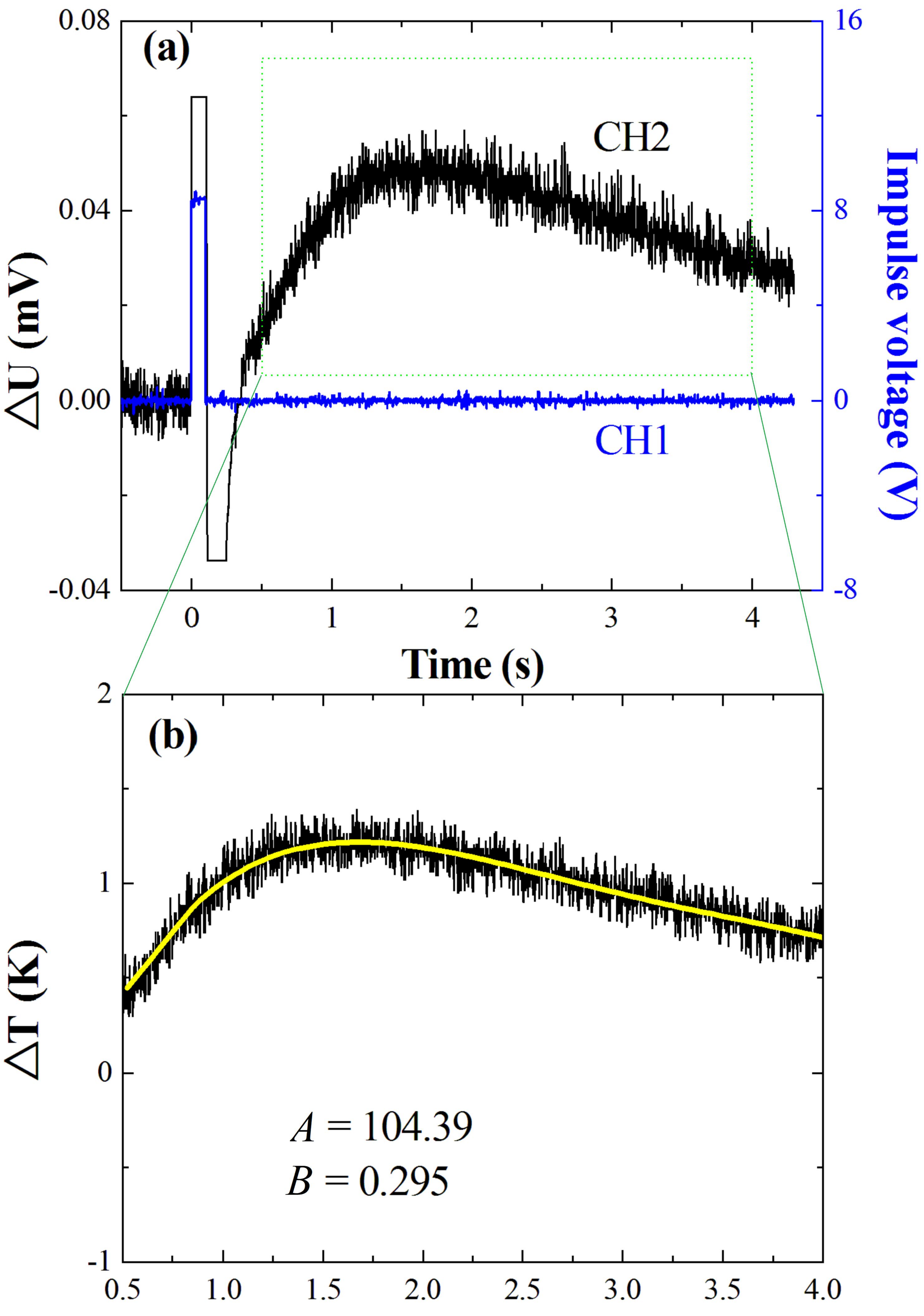
(a)
CH2
CH1
ΔU (mV)
Impulse voltage (V)
0.08
0.04
0.00
-0.04
16
8
0
-8
0
1
2
3
4
Time (s)
(b)
ΔT (K)
A = 104.39
B = 0.295
2
1
0
-1
0.5
1.0
1.5
2.0
2.5
3.0
3.5
4.0
Time (s)

Fig. 3

(a)

P = 0.5 GPa

Syenogranite
Alkaline granite
Monzogranite
Granodiorite

Thermal diffusivity (mm^2s^{-1})

Temperature (K)

(b)

P = 0.5 GPa

Syenogranite
Alkaline granite
Monzogranite
Granodiorite

Thermal conductivity ($Wm^{-1}K^{-1}$)

Temperature (K)

(c)

300 K

900 K

600 K

Alkaline granite
Syenogranite
Monzogranite
Granodiorite
Monzogranite
Granodiorite

Thermal diffusivity (mm^2s^{-1})

Pressure (GPa)

(d)

300 K

900 K

600 K

Alkaline granite
Syenogranite
Monzogranite
Granodiorite
Monzogranite
Granodiorite

Thermal conductivity ($Wm^{-1}K^{-1}$)

Pressure (GPa)

Fig. 4

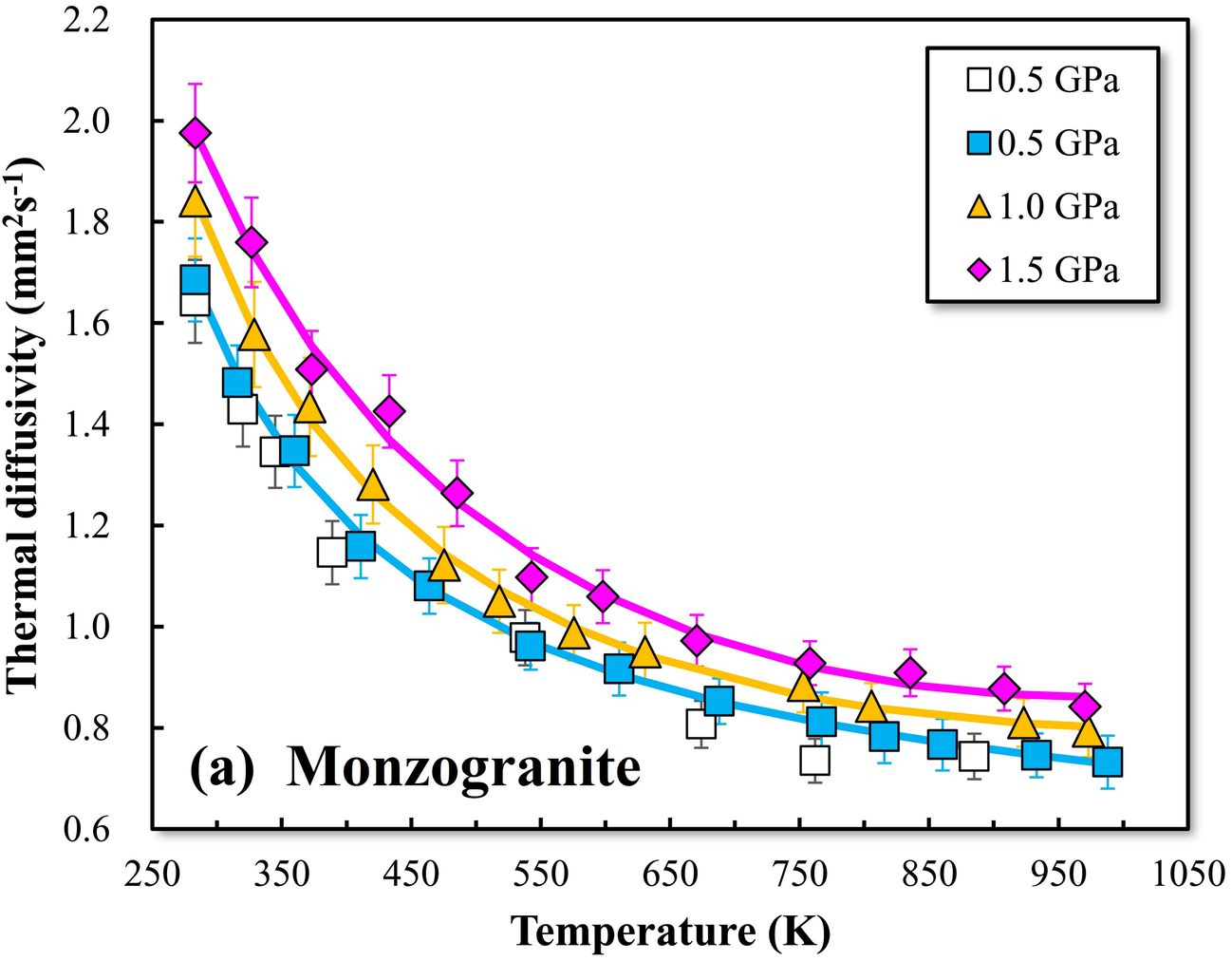
0.5 GPa
0.5 GPa
1.0 GPa
1.5 GPa
(a) Monzogranite
Thermal diffusivity (mm²s⁻¹)
Temperature (K)

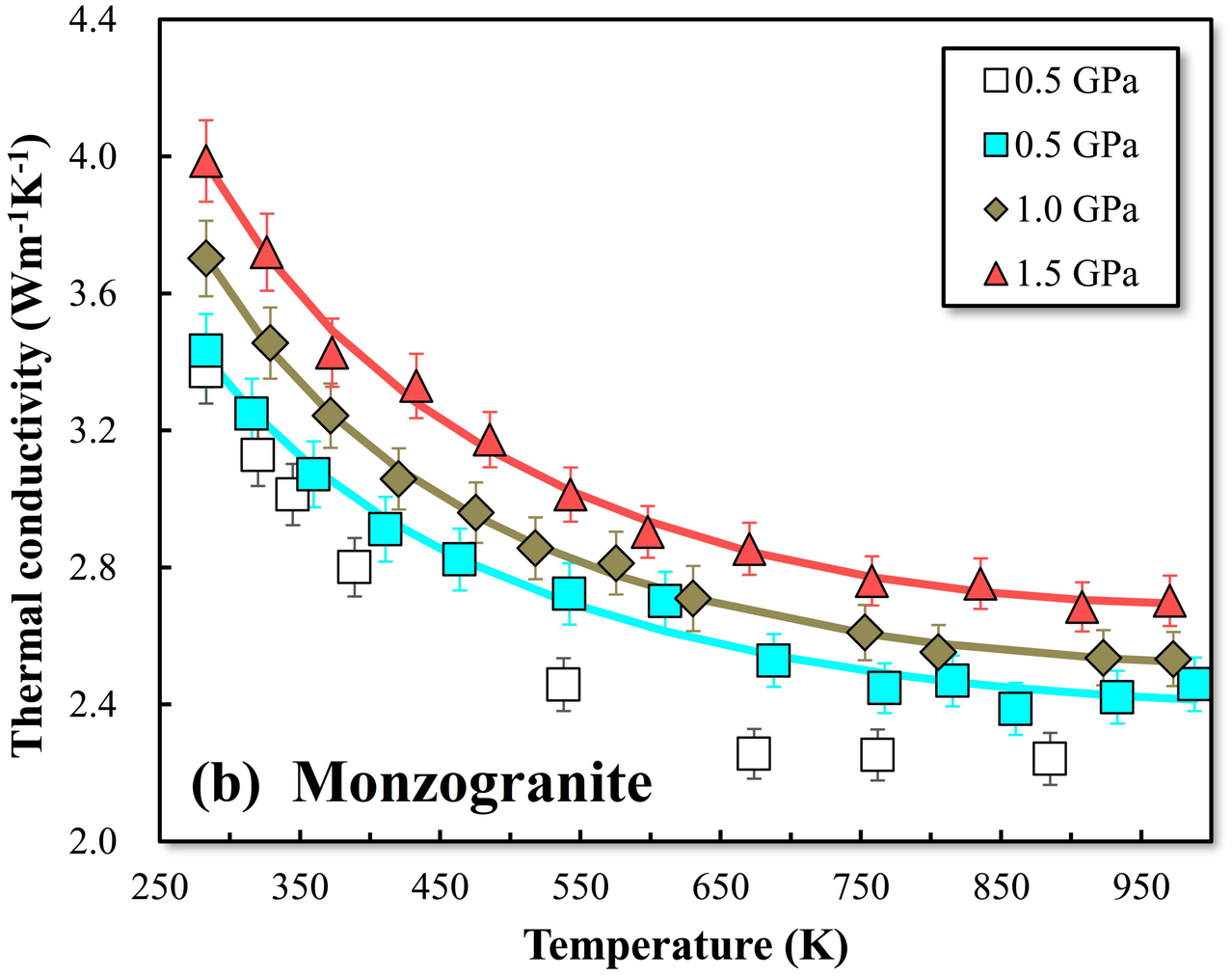
0.5 GPa
0.5 GPa
1.0 GPa
1.5 GPa
(b) Monzogranite
Thermal conductivity (Wm⁻¹K⁻¹)
Temperature (K)

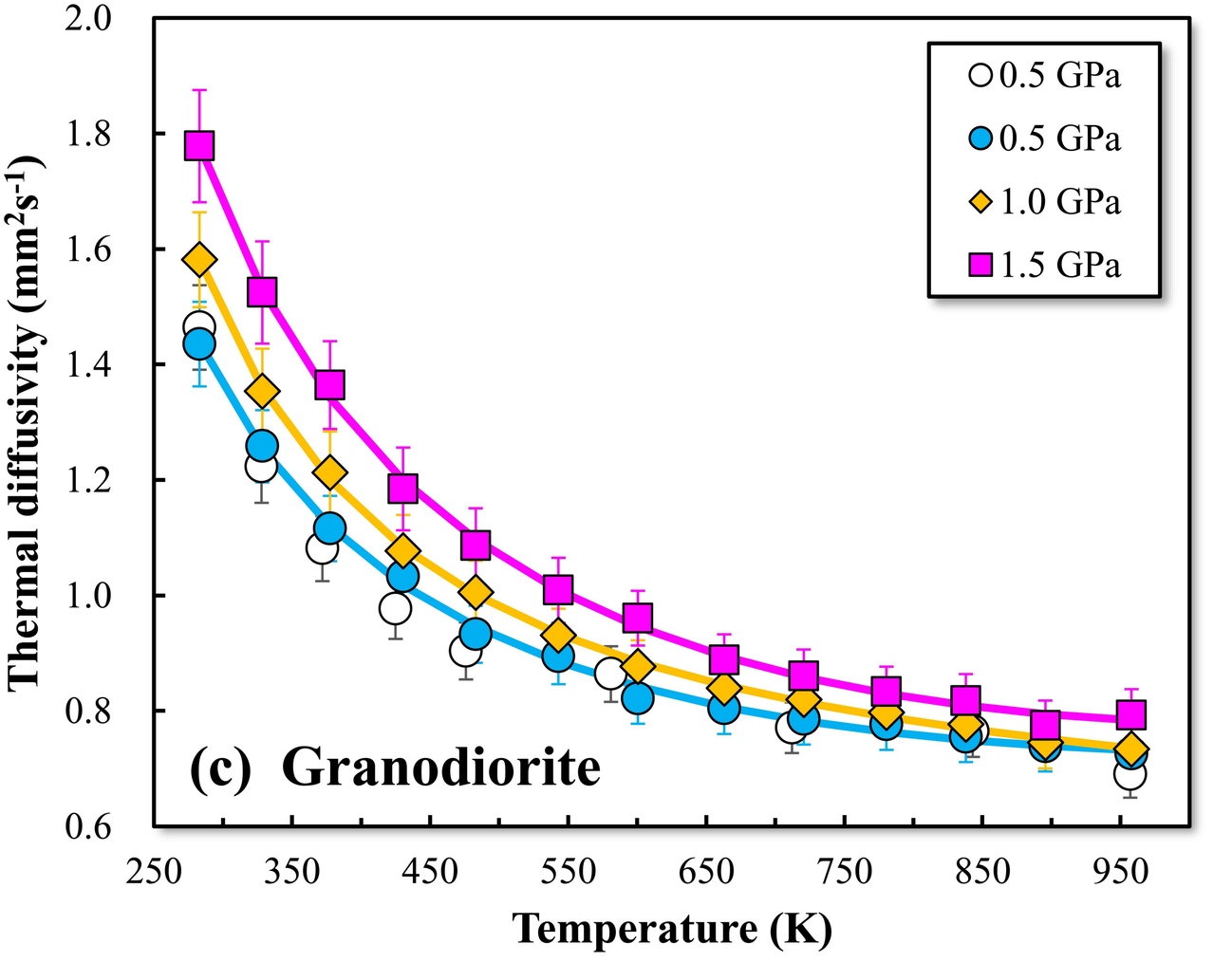
0.5 GPa
0.5 GPa
1.0 GPa
1.5 GPa
(c) Granodiorite
Thermal diffusivity (mm²s⁻¹)
Temperature (K)

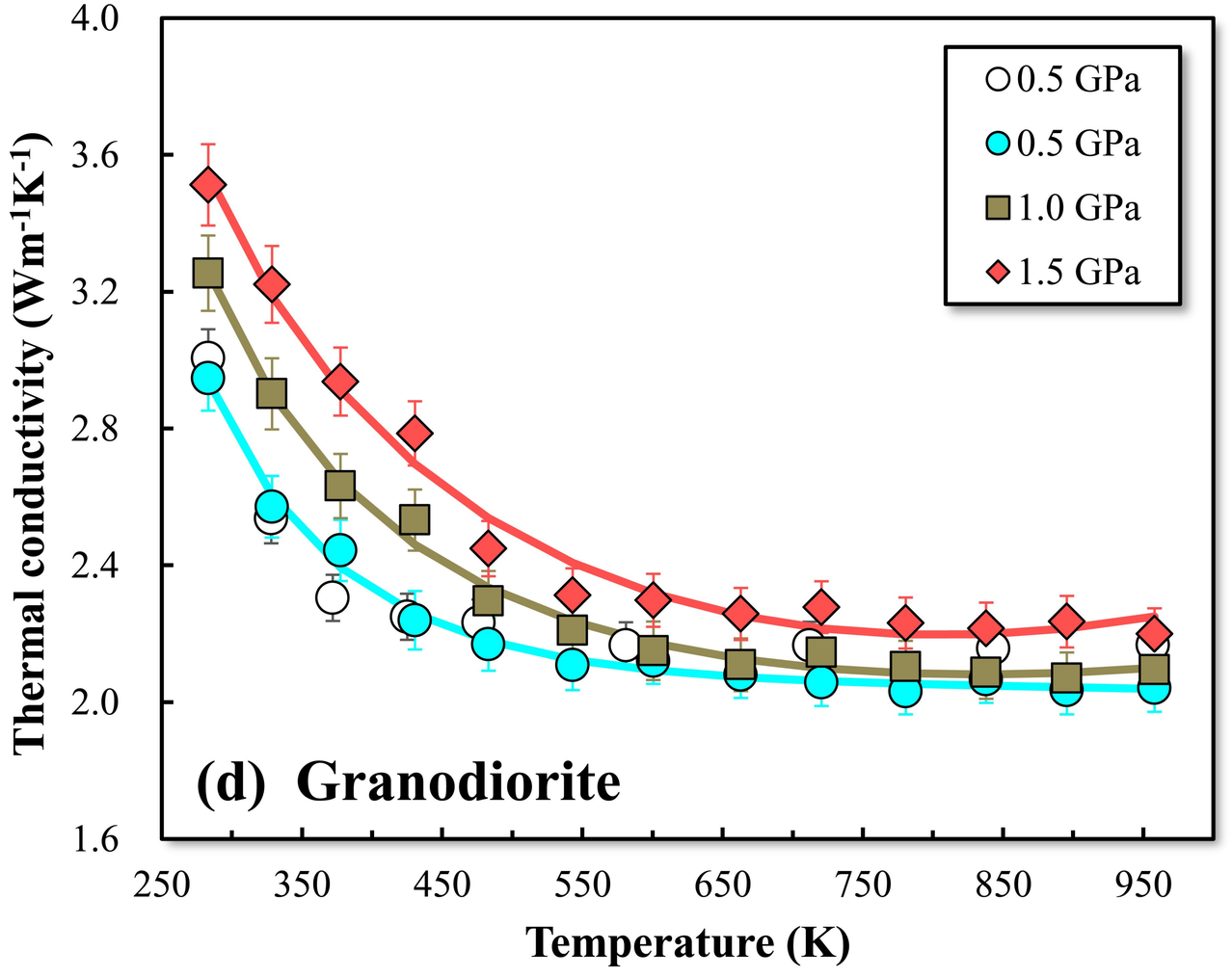
0.5 GPa
0.5 GPa
1.0 GPa
1.5 GPa
(d) Granodiorite
Thermal conductivity (Wm⁻¹K⁻¹)
Temperature (K)

Fig. 5

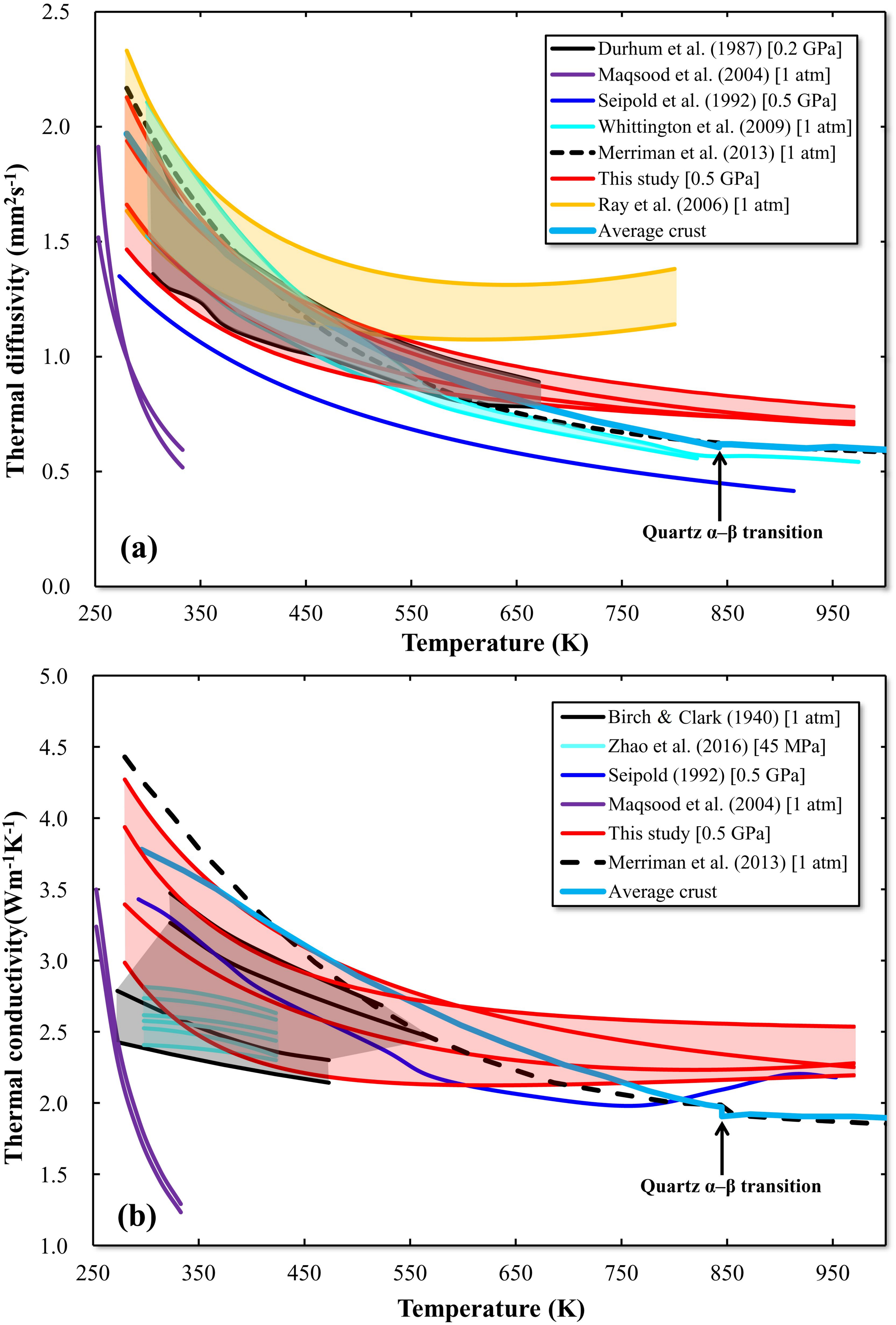
Thermal diffusivity (mm²s⁻¹)
2.5
2.0
1.5
1.0
0.5
0.0
250
350
450
550
650
750
850
950
Temperature (K)
Durhum et al. (1987) [0.2 GPa]
Maqsood et al. (2004) [1 atm]
Seipold et al. (1992) [0.5 GPa]
Whittington et al. (2009) [1 atm]
Merriman et al. (2013) [1 atm]
This study [0.5 GPa]
Ray et al. (2006) [1 atm]
Average crust
Quartz α–β transition
(a)
Thermal conductivity(Wm⁻¹K⁻¹)
5.0
4.5
4.0
3.5
3.0
2.5
2.0
1.5
1.0
250
350
450
550
650
750
850
950
Temperature (K)
Birch & Clark (1940) [1 atm]
Zhao et al. (2016) [45 MPa]
Seipold (1992) [0.5 GPa]
Maqsood et al. (2004) [1 atm]
This study [0.5 GPa]
Merriman et al. (2013) [1 atm]
Average crust
Quartz α–β transition
(b)

Fig. 6

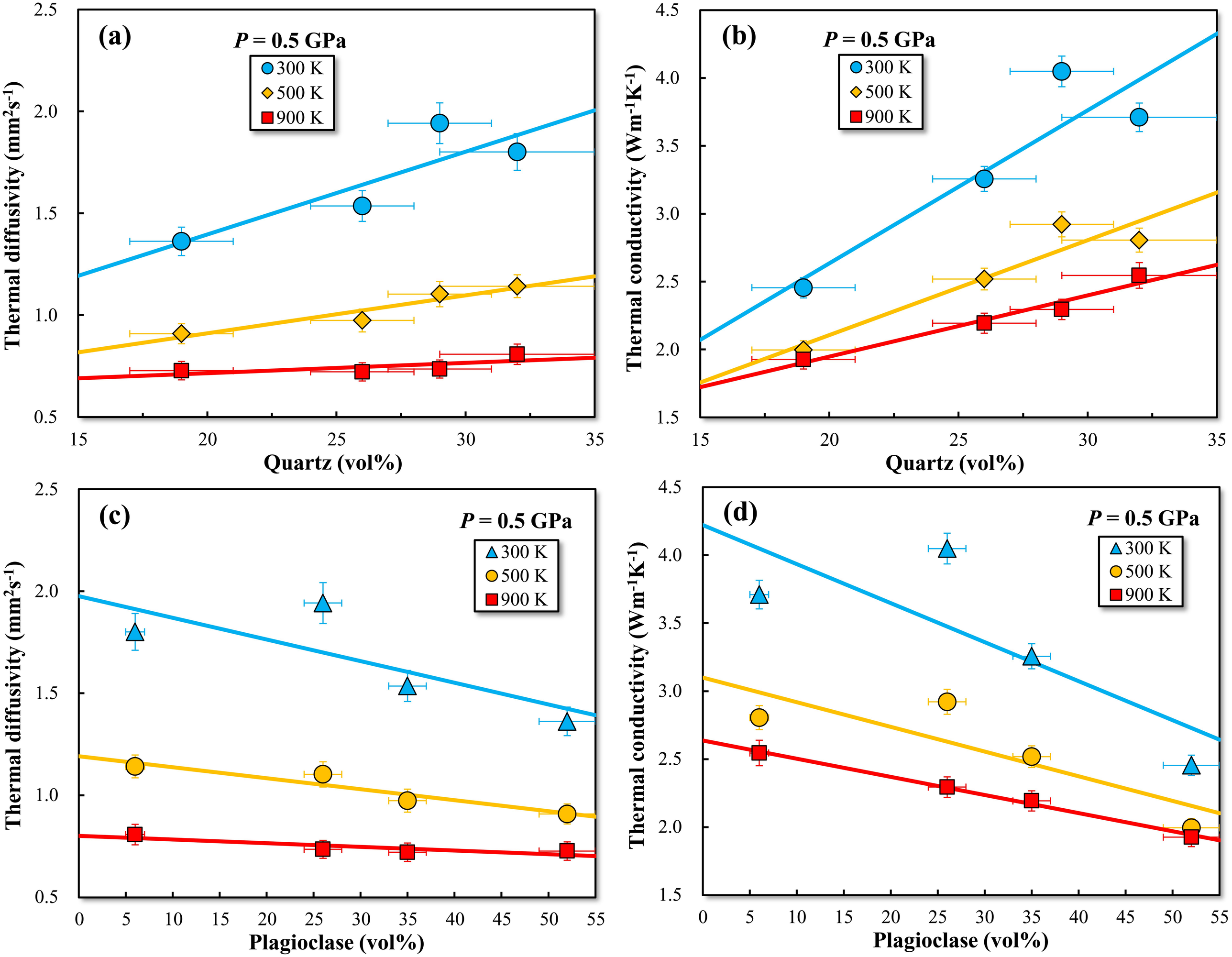
(a)
P = 0.5 GPa
300 K
500 K
900 K
Thermal diffusivity (mm²s⁻¹)
Quartz (vol%)
(b)
P = 0.5 GPa
300 K
500 K
900 K
Thermal conductivity (Wm⁻¹K⁻¹)
Quartz (vol%)
(c)
P = 0.5 GPa
300 K
500 K
900 K
Thermal diffusivity (mm²s⁻¹)
Plagioclase (vol%)
(d)
P = 0.5 GPa
300 K
500 K
900 K
Thermal conductivity (Wm⁻¹K⁻¹)
Plagioclase (vol%)

Fig. 7

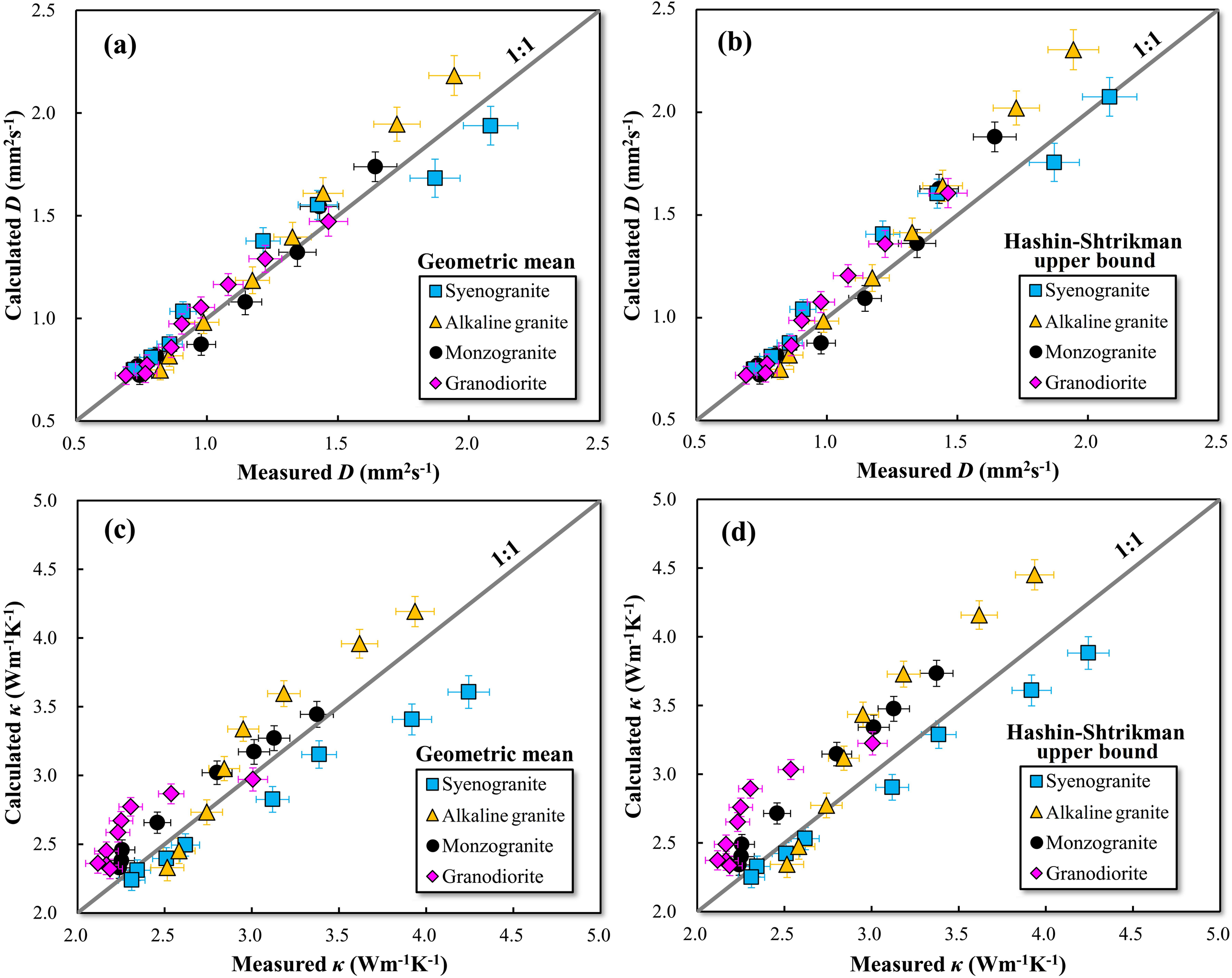
(a)
1:1
Geometric mean
Syenogranite
Alkaline granite
Monzogranite
Granodiorite
Calculated D (mm²s⁻¹)
Measured D (mm²s⁻¹)
(b)
1:1
Hashin-Shtrikman upper bound
Syenogranite
Alkaline granite
Monzogranite
Granodiorite
Calculated D (mm²s⁻¹)
Measured D (mm²s⁻¹)
(c)
1:1
Geometric mean
Syenogranite
Alkaline granite
Monzogranite
Granodiorite
Calculated κ (Wm⁻¹K⁻¹)
Measured κ (Wm⁻¹K⁻¹)
(d)
1:1
Hashin-Shtrikman upper bound
Syenogranite
Alkaline granite
Monzogranite
Granodiorite
Calculated κ (Wm⁻¹K⁻¹)
Measured κ (Wm⁻¹K⁻¹)

Fig. 8

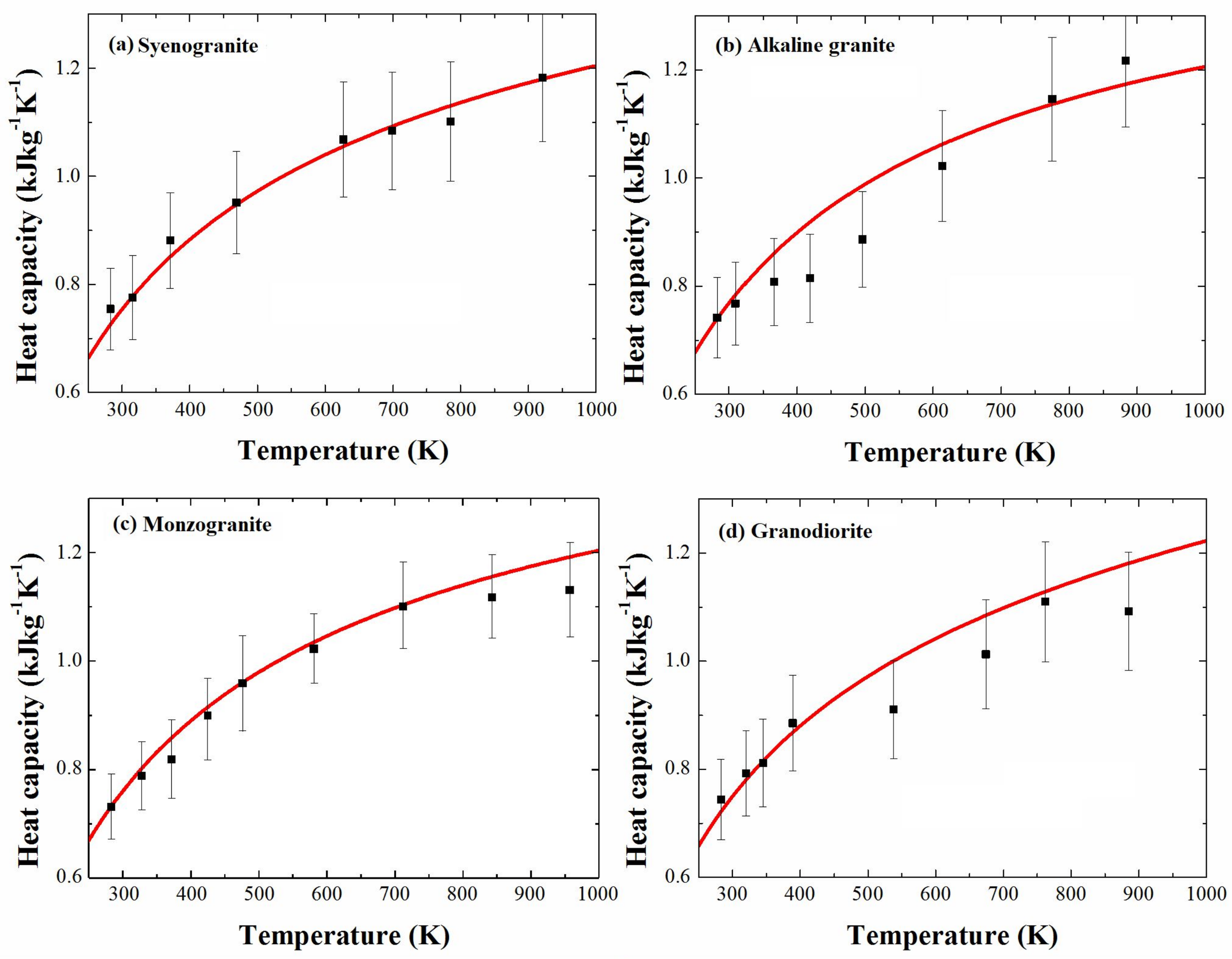
(a) Syenogranite
(b) Alkaline granite
(c) Monzogranite
(d) Granodiorite
Heat capacity (kJkg-1K-1)
Temperature (K)
0.6
0.8
1.0
1.2
300
400
500
600
700
800
900
1000

Fig. 9

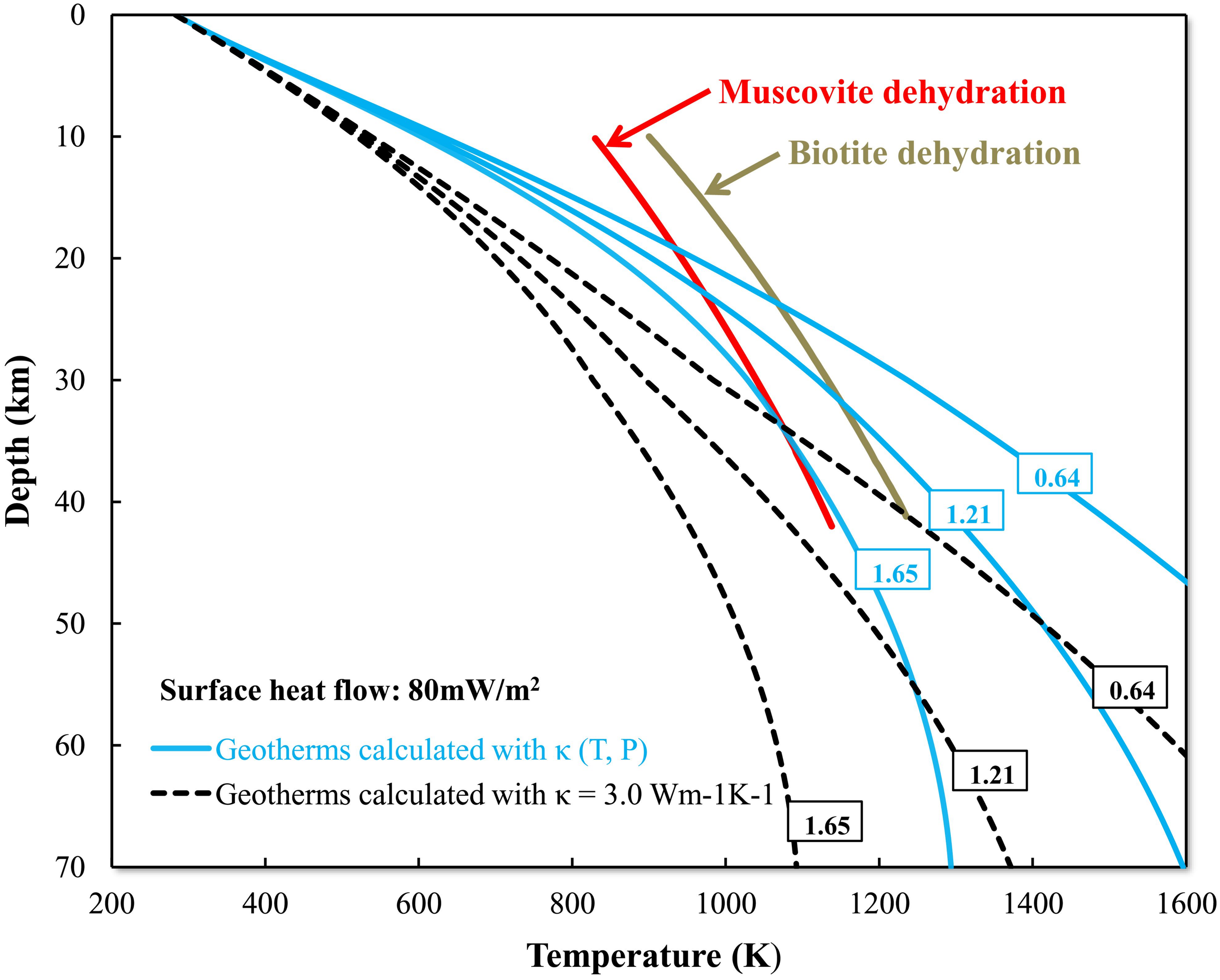
Muscovite dehydration
Biotite dehydration
0.64
1.21
1.65
0.64
1.21
1.65
Surface heat flow: 80mW/m²
Geotherms calculated with κ (T, P)
Geotherms calculated with κ = 3.0 Wm-1K-1
Depth (km)
Temperature (K)
0
10
20
30
40
50
60
70
200
400
600
800
1000
1200
1400
1600

Fig. 10